

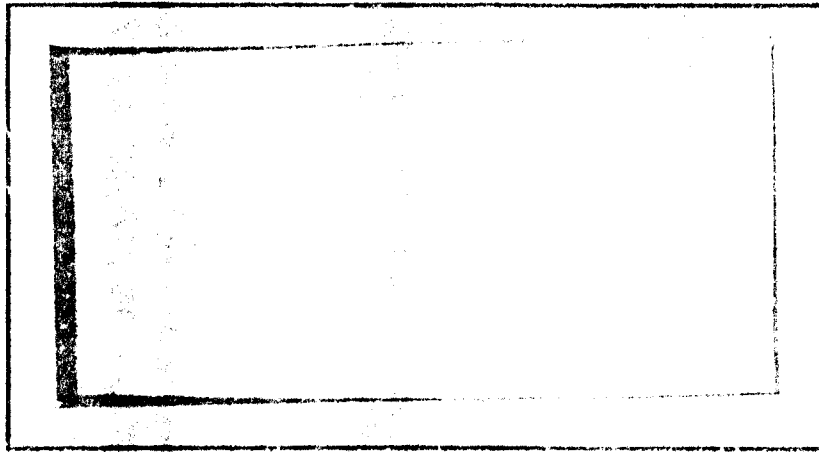
AO 48370

1

AIR FORCE INSTITUTE OF TECHNOLOGY



AIR UNIVERSITY
UNITED STATES AIR FORCE



D. D. D.
JAN 16 1918

Best Available Copy

SCHOOL OF ENGINEERING

WRIGHT-PATTERSON AIR FORCE BASE, OHIO

AD No. _____
ODG FILE COPY

Approved for Distribution
Distribution Statement

①

20
JAN 10 1977
AFIT/AA/77D-15

AN EXPERIMENTAL INVESTIGATION
OF STEADY ASYMMETRIC VORTEX SHEDDING
FROM A SLENDER BODY OF REVOLUTION AT
HIGH ANGLES OF ATTACK

THESIS

AFIT/GAE/AA/77D-15 Robert R. Turelli
Captain USAF

Preface

The purpose of this study was to determine experimentally the effects of Mach number and Reynolds number on the large side forces which occur on a slender body of revolution at high angles of attack due to asymmetric vortex formation and shedding. In addition to the experimental study, an AFFDL empirical prediction program was utilized to compare predicted normal and side forces to those determined experimentally.

I wish to thank my thesis advisor, Capt. Richard A. Merz, for his guidance and support throughout the project and for bringing this thesis topic to my attention.

I also wish to thank and acknowledge the outstanding craftsmanship of Mr. Carl Short and Mr. Russ Murry of the AFIT Model Fabrication Division for the excellent model which they produced.

I would also like to thank the following individuals of the Aeromechanics Division, Air Force Flight Dynamics Laboratory: Mr. Noel Allen, Mr. Ed Robinson, Mr. Joe Martin, and Capt. Tracy Rhodes for their support throughout the test phase; Mr. Valentine H. Dahlem for his guidance and assistance throughout the project; and Mr. Jack I. Flaherty and Mr. Donald E. Shereda for their computer programming assistance.

Finally, I would like to give a special thanks to my wife, Diane, not only for typing this thesis but also for

her patience and understanding throughout the past 18
months.

Robert R. Turelli

Table of Contents

	<u>Page</u>
Preface	ii
List of Figures	v
List of Symbols	vii
Abstract	viii
I. Introduction	1
II. Test Facility and Model Description	3
III. Experimental Procedures	6
IV. Empirical Program	8
V. Results and Discussion	9
VI. Conclusions and Recommendations	14
VII. Figures	17
Bibliography	50
Vita	52

List of Figures

<u>Figure</u>		<u>Page</u>
1	Steady, Symmetric Vortices	17
2	Steady, Asymmetric Vortices	18
3	Model Pressure Orifice Location	19
4	Axisymmetric Model Tested	20
5	Model and Support Section	20
6	Model and Support Section Installed in TGF . .	21
7	Circumferential Pressure Distributions	22
8	Circumferential Pressure Distributions	23
9	Circumferential Pressure Distributions	24
10	Effect of Mach Number on Local Side and Normal Force Coefficients at $Re_D = 41,667$	25
11	Effect of Mach Number on Local Side and Normal Force Coefficients at $Re_D = 83,333$	26
12	Effect of Mach Number on Local Side Force Coefficient at $Re_D = 166,667$	27
13	Effect of Mach Number on Local Normal Force Coefficient at $Re_D = 166,667$	28
14	Effect of Reynolds Number on Local Side and Normal Force Coefficients at $M = .3$	29
15	Effect of Reynolds Number on Local Side and Normal Force Coefficients at $M = .4$	30
16	Effect of Reynolds Number on Local Side and Normal Force Coefficients at $M = .5$	31
17	Effect of Reynolds Number on Local Side and Normal Force Coefficients at $M = .6$	32
18	Effect of Reynolds Number on Local Side and Normal Force Coefficients at $M = .7$	33
19	Effect of Reynolds Number on Local Side and Normal Force Coefficients at $M = .8$	34

<u>Figure</u>	<u>Page</u>
20 Experimental and Predicted Local Normal Force Coefficients at $M = .3$	35
21 Experimental and Predicted Local Normal Force Coefficients at $M = .4$	36
22 Experimental and Predicted Local Normal Force Coefficients at $M = .5$	37
23 Experimental and Predicted Local Normal Force Coefficients at $M = .6$	38
24 Experimental and Predicted Local Normal Force Coefficients at $M = .7$	39
25 Experimental and Predicted Local Normal Force Coefficients at $M = .8$	40
26 Experimental and Predicted Local Side Force Coefficients at $M = .3$	41
27 Experimental and Predicted Local Side Force Coefficients at $M = .4$	42
28 Experimental and Predicted Local Side Force Coefficients at $M = .5$	43
29 Experimental and Predicted Local Side Force Coefficients at $M = .6$	44
30 Experimental and Predicted Local Side Force Coefficients at $M = .7$	45
31 Experimental and Predicted Local Side Force Coefficients at $M = .8$	46
32 Oil Flow at $Re_D = 41,667$ $M = .4$ $\alpha = 45^\circ$. . .	47
33 Oil Flow at $Re_D = 83,333$ $M = .3$ $\alpha = 45^\circ$. . .	47
34 Oil Flow at $Re_D = 83,333$ $M = .6$ $\alpha = 45^\circ$. . .	48
35 Oil Flow at $Re_D = 166,667$ $M = .3$ $\alpha = 30^\circ$. .	48
36 Oil Flow at $Re_D = 166,667$ $M = .3$ $\alpha = 45^\circ$. .	49

List of Symbols

Alpha, α	Angle of Attack
C_N	Local Normal Force Coefficient
C_P	Pressure Coefficient, $(P - P_\infty)/(\frac{1}{2}\rho_\infty U_\infty^2)$
C_Y	Local Side Force Coefficient
D	Reference Diameter of Missile Based on Cylindrical Afterbody Diameter
L_B	Afterbody Length
L_N	Nose Length
M	Mach Number
P_∞	Free Stream Static Pressure
Phi, ϕ	Circumferential Pressure Tap Location in Degrees
r	Radius of Cylindrical Afterbody
Re	Reynolds Number
Re_D	Reynolds Number Based on Reference Diameter
S	Afterbody Cross Sectional Area, πr^2
U_∞	Free Stream Velocity
X	Axial Location Measured From Tip of Nose
ρ_∞	Free Stream Density

Abstract

An experimental investigation of the effects of Mach number and Reynolds number on the side forces induced on a slender body of revolution at high angles of attack was conducted. The tests were carried out in the Air Force Flight Dynamics Laboratory's Trisonic Gasdynamic Facility. The model tested consisted of a sharp, tangent ogive nose of fineness ratio $L_N/D = 3.0$ followed by a cylindrical afterbody of fineness ratio $L_B/D = 7.5$. The model was tested at unit Reynolds numbers of 0.5×10^6 , 1.0×10^6 , and 2.0×10^6 per foot, Mach numbers between 0.3 and 0.8, and angles of attack between 27 and 45 degrees. From the pressure data, local side and normal force coefficients were calculated. These were compared to predicted local side and normal force coefficients using a current state of the art method. The results of the tests indicated that Mach and Reynolds numbers had a significant effect on C_N and C_Y . Increasing Mach number decreased the magnitude of C_Y , while increasing Reynolds number increased the magnitude of C_Y . The effect of Mach and Reynolds numbers on the magnitude of C_N depended on the particular flow conditions. No general trends were established. The predicted values of C_N and C_Y did not compare well with the values of C_N and C_Y obtained experimentally.

AN EXPERIMENTAL INVESTIGATION
OF STEADY ASYMMETRIC VORTEX SHEDDING
FROM A SLENDER BODY OF REVOLUTION AT
HIGH ANGLES OF ATTACK

I. Introduction

A slender axisymmetric body moving through a real fluid experiences four distinct flow patterns depending on its angle of attack relative to the free stream (Refs 1-2). For angles of attack in the range of 0 to 5 degrees, the flow does not separate and can be described by a potential flow field and an attached laminar or turbulent boundary layer. At angles of attack ranging from 5 to 25 degrees, separation occurs and a steady, symmetric vortex pair is shed (Fig 1). As a consequence, no side force exists. At angles of attack between 25 and 50 degrees, the symmetric vortex cores become asymmetric and break away from the sides of the body at different axial locations (Fig 2). This steady, asymmetrical flow field produces a considerable side force, especially at subsonic speeds. As the angle of attack increases to between 50 and 70 degrees, the flow field becomes unsteady as the vortex cores randomly switch from side to side. Finally, above an angle of attack of 70 degrees, the flow pattern degenerates into a completely turbulent wake.

It has been observed (Refs 3-7) that Mach number, Reynolds number, angle of attack, nose fineness ratio and nose bluntness all affect the side force characteristics.

It has also been shown (Refs 3-7) that the magnitude of the side force is extremely sensitive to model nose misalignment. In fact, the formation of an asymmetric vortex pattern is believed to be caused by very small asymmetries in the nose (Refs 3-7).

The objective of this wind tunnel investigation was to determine the effects of Mach and Reynolds numbers on the magnitudes of the normal and side forces which occur on a slender body of revolution at angles of attack between 27 and 45 degrees (steady, asymmetric vortex shedding). Mach numbers and unit Reynolds numbers were varied between 0.3 and 0.8 and between 0.5×10^6 and 2.0×10^6 per foot, respectively. In addition to the experimental study, an AFFDL digital computer program was used to predict the normal and side forces. These predicted values were compared to the values determined experimentally.

II. Test Facility and Model Description

The experimental testing was conducted in the Air Force Flight Dynamics Laboratory's (AFFDL) Trisonic Gasdynamic Facility (TGF) located at Wright-Patterson Air Force Base. The TGF is a closed circuit, variable density, continuous flow wind tunnel capable of operating within a Mach number range of 0.23 to 4.76 and within a unit Reynolds number range of approximately 0.25×10^6 to 5.85×10^6 per foot. Two 28 inch diameter hinged windows mounted on the wind tunnel walls provided access to the test section and an unobstructed view of the model. The windows made possible the use of schlieren optical test equipment and an oil flow visualization technique. The model and sting were supported by a rack mounted fifty-inch radius crescent with a pitch range of -1 to 19 degrees, $\pm .01$ degrees. The center of rotation coincided with the center of the test section viewing window. A more detailed description of the tunnel and its operating conditions can be found in Ref 8.

The one inch diameter model, illustrated in Fig 3, consisted of a sharp, tangent ogive nose of fineness ratio $L_N/D = 3.0$ followed by a cylindrical afterbody of fineness ratio $L_B/D = 7.5$. The size of the model was principally determined by the desire to keep body and wake blockage effects to less than 1%. To obtain pressure readings, the model was instrumented with 84 pressure orifices located at six axial stations on the cylinder (Fig 3).

The total number of pressure orifices was limited to the number of pressure tubes that could physically fit inside the model without adopting a tube diameter too small for accurate pressure measurements. The six axial stations were located 3.5 to 7.0 model diameters aft of the nose tip. These locations were chosen in order to cover the area in which the maximum local side force was expected to occur. This area was determined from data obtained by AFFDL in tests on the MX advanced ICBM weapon system (Ref 9). At each axial station, pressure taps were located as indicated in Fig 3. This particular distribution was chosen in order to obtain more accurate pressure distributions in the separated flow region. Flow around the lower 120 degrees of the cylinder remained attached and was assumed to be a region characterized by potential flow.

After being attached to the model, the tubes were passed through the support section, routed out of the tunnel and connected to two 48-port scanivalves. Each scanivalve contained a Statham pressure transducer which was used as the primary pressure sensing instrument. The data obtained from the transducers were accurate to $\pm 0.2\%$. Data reduction was accomplished by feeding the signals from the pressure transducers to a Control Data Corporation (CDC) 6600 digital computer. For each axial station, the computer listed the pressure coefficients and plotted these values versus angular pressure tap

location.

In order to traverse the 27 to 45 degree angle of attack range studied, a constant diameter support section was designed and constructed to fit into the tunnel rack mounted fifty inch radius crescent. The length of the sting was such that the model body center location coincided with the center of rotation of the crescent.

Photographs of the model, support section, and model and support section installed in the tunnel have been presented in Figs 4 through 6.

III. Experimental Procedures

The experimental testing was divided into two phases. The first phase consisted of collecting detailed surface pressure measurements at free stream Mach numbers between 0.3 and 0.8 and angles of attack ranging from 27 to 45 degrees. The free stream unit Reynolds number was varied from 0.5×10^6 to 2.0×10^6 per foot. This resulted in Reynolds numbers based on model diameter of 0.42×10^5 to 1.67×10^5 . Pressure coefficients based on free stream static pressure and tunnel dynamic pressure were listed and plotted versus angular pressure tap location for each axial station. This was accomplished during the test via the CDC 6600 digital computer. These pressure coefficients were then used to calculate the local side and normal force coefficients.

The second phase consisted of flow visualization studies. Two techniques were applied. A Z-type schlieren system was used to view flow field patterns and vortex lines. An oil flow, made up of STP and titanium oxide powder brushed on the model, was used to show the interaction between streamlines and to indicate regions of flow separation. The schlieren photos were taken simultaneously with the pressure measurements, while the oil flow study was accomplished after all pressure measurements were completed.

During the first phase, it was observed that the model produced a steady, symmetric vortex pattern. In order to

III. Experimental Procedures

The experimental testing was divided into two phases. The first phase consisted of collecting detailed surface pressure measurements at free stream Mach numbers between 0.3 and 0.8 and angles of attack ranging from 27 to 45 degrees. The free stream unit Reynolds number was varied from 0.5×10^6 to 2.0×10^6 per foot. This resulted in Reynolds numbers based on model diameter of 0.42×10^5 to 1.67×10^5 . Pressure coefficients based on free stream static pressure and tunnel dynamic pressure were listed and plotted versus angular pressure tap location for each axial station. This was accomplished during the test via the CDC 6600 digital computer. These pressure coefficients were then used to calculate the local side and normal force coefficients.

The second phase consisted of flow visualization studies. Two techniques were applied. A Z-type schlieren system was used to view flow field patterns and vortex lines. An oil flow, made up of STP and titanium oxide powder brushed on the model, was used to show the interaction between streamlines and to indicate regions of flow separation. The schlieren photos were taken simultaneously with the pressure measurements, while the oil flow study was accomplished after all pressure measurements were completed.

During the first phase, it was observed that the model produced a steady, symmetric vortex pattern. In order to

induce a steady, asymmetric vortex pattern, a vortex generator was placed on one side of the nose. The vortex generator consisted of a 1/8 inch wide, 1/2 inch long strip of No. 80 silicone carbide crystals. The generator was located at the 90 degree point of the nose and 1.25 to 1.75 inches aft of the nose tip. The generator insured that a maximum side force would occur on the model. Schlieren photographs were taken with and without the vortex generator. Oil flow pictures of the model were taken only with the vortex generator.

It should be noted that for both grit and no-grit nose configurations, several test runs were repeated at selected Reynolds numbers, Mach numbers, and angles of attack. The agreement between the initial and the repeated test data was within $\frac{1}{2}\%$, indicating that the data was repeatable.

IV. Empirical Program

The original version of Andrew B. Wardlaw's (Ref 7) digital computer program was used to predict the normal and side forces acting on the model. Wardlaw's multivortex model of asymmetric vortex shedding is based on the impulsive flow analogy (Ref 10). In this technique, a large number of point vortices are superimposed on the potential solution for flow about a cylinder in order to simulate the viscous crossflow plane. The asymmetric flow field is developed by initially perturbing the solution. Gothert's Rule is then applied to account for compressibility effects. The total force acting on the model is assumed to be the sum of a viscous part obtained from the crossflow analogy and an inviscid part obtained from slender body theory.

The digital program required the input of the following parameters: angle of attack, Mach number, free stream Reynolds number based on model diameter, and nose and body geometries. Modifications to the program are presently being made by AFFDL.

V. Results and Discussion

Coefficients of pressure based on tunnel dynamic pressure were plotted versus angular pressure tap location. This was accomplished at each axial station for both grit and no-grit nose configurations. An example of a circumferential pressure distribution is presented in Fig 7. The pressure peaks on the plot indicate the presence of separated vortex filaments. At a 27 degree angle of attack, the pressure distribution is symmetrical. For larger angles of attack, the asymmetric pressure distribution indicates an asymmetric vortex development.

Plots of circumferential pressure distributions were compared for both grit and no-grit nose configurations. Figures 8 and 9 illustrate typical pressure distributions. It was observed that the addition of the grit vortex generator on the nose of the model had a significant effect on the symmetry of the pressure distributions, as was expected. For the no-grit model, asymmetries in the pressure distributions were observed only at angles of attack between 40 and 45 degrees and only at free stream unit Reynolds numbers of 1.0×10^6 and 2.0×10^6 per foot. The absence of asymmetry in the no-grit circumferential pressure distributions was attributed to a model nose that was very symmetrical in shape and/or to the roll angle at which the model was tested.

With the application of the grit vortex generator

U
on the nose, the pressure distributions became asymmetric at nearly all test conditions. Also, the magnitudes of the local side force coefficients were found to be greater than previously observed (Figs 8 - 9). This was expected since the grit was added to the nose in order to force a steady, asymmetric vortex pattern and a maximum side force. The above observations indicated that the magnitude of the local side force coefficient was extremely sensitive to nose asymmetries. This has been confirmed by other investigators (Refs 1 - 7).

Local normal and side force coefficients were calculated from the experimental pressure distributions by integrating around the model circumference and along the axial direction from $X/D = 3.5$ to $X/D = 7.0$ using the following formulae (Ref 11:3):

$$C_N = (1/S) \iint C_P \cos\phi \, r \, dx \, d\phi \quad \dots(1)$$

$$C_Y = (1/S) \iint C_P \sin\phi \, r \, dx \, d\phi \quad (2)$$

Since this study was interested in maximum local side force coefficients, experimental values of C_Y and C_N were calculated for the nose with grit configuration only.

Theoretical values of C_N and C_Y were obtained by integrating the predicted axial station normal and side force coefficients along the axial direction from $X/D = 3.5$ to $X/D = 7.0$.

Plots of the experimental values of C_N and C_Y versus angle of attack are presented in Figs 10 through 19. It should be noted that the absolute magnitudes of the local

side force coefficients were plotted versus angle of attack. This eliminated the additional complication of local side force direction. The plots show that, in general, increasing the angle of attack increased the magnitudes of C_N and C_Y . The maximum value of C_N occurred at an angle of attack of 45 degrees for all flow conditions while the maximum value of C_Y varied between 35 and 45 degrees angle of attack, depending on the particular flow condition.

In Figs 10 through 13, data are presented to show the effect of Mach number on C_N and C_Y . In general, as Mach number increased, C_Y decreased. This result was found to be in agreement with the results of other investigators (Ref 1 - 5). At constant Reynolds numbers, C_N was significantly affected by the free stream Mach number. At $Re_D = 41,667$ and $M \geq 0.5$, C_N increased with increasing Mach number at all angles of attack. The largest values of C_N at this Reynolds number for all angles of attack occurred at $M = 0.4$. For $Re_D = 83,333$ and $Re_D = 166,667$, C_N generally decreased with increasing Mach number for angles of attack greater than 35 degrees. At angles of attack less than 35 degrees, no clear trends were established.

In Figs 14 through 19, data are presented to show the effect of Reynolds number on C_N and C_Y . In general, C_Y increased with increasing Reynolds number. This result was in agreement with the results presented by Fleeman and Nelson (Ref 12) who observed that side force increased up to $Re_D = 2.5 \times 10^5$ and then decreased with increasing

Reynolds number. For angles of attack above 35 degrees and $M \geq 0.5$, C_N increased with increasing Reynolds number. For all other angles of attack and Mach numbers, no general trends were observed.

Figures 20 through 25 compare the experimental and predicted local normal force coefficients. At angles of attack less than or equal to 30 degrees, predicted values of C_N underestimated the experimental values, while at angles of attack greater than or equal to 35 degrees, predicted values overestimated experimental ones. The theoretical and experimental curves crossed between 30 and 35 degrees.

Figures 26 through 31 compare the experimental and predicted local side force coefficients. At both $Re_D = 83,333$ and $Re_D = 166,667$ for $M \leq 0.5$, the theory overestimated the experimental values of C_Y for angles of attack less than or equal to 30 degrees and underestimated the experimental values of C_Y for angles of attack greater than or equal to 37 degrees. The two curves crossed between 30 and 37 degrees. For $M \geq 0.6$ and the same Reynolds numbers, the theory overestimated the values of C_Y for all angles of attack. For $Re_D = 41,667$, the theory overestimated the values of C_Y for all Mach numbers and angles of attack.

The theory also failed to correctly account for the increase in the magnitude of C_Y with increasing Reynolds number and the decrease in the magnitude of C_Y with

0
increasing Mach number. The theory did correctly simulate the general effect of Mach and Reynolds number on C_N in comparison with those effects determined experimentally.

Flow Visualization

Due to the small density gradients that existed across vortex lines, it was impossible to distinguish the vortex cores from the background noise in the schlieren photographs. Although the vortex cores could not be photographed, they were at times visible when the flow field was viewed through the optical system. The oil flow visualization technique, however, did show the streamline interactions and the regions of flow separation. Examples are presented in Figs 32 through 36. It was observed that flow separation occurred between the 85 to 95 degree points on the cylinder over its entire length for all test conditions run.

VI. Conclusions and Recommendations

Conclusions

Results from wind tunnel tests on a slender axisymmetric body composed of a sharp, tangent ogive nose followed by a cylindrical afterbody have been presented. Surface pressure distributions were obtained over a wide range of Mach and Reynolds numbers and from these the local side and normal force coefficients were calculated. The original version of Wardlaw's digital computer program was used to predict the local normal and side force coefficients. From an analysis of the data obtained and a comparison of the predicted and experimental values of C_N and C_Y , the following can be concluded:

1. Applying a grit vortex generator on the nose of the model produces a steady, asymmetrical flow field.
2. The magnitude of the local side force coefficient is extremely sensitive to nose asymmetries.
3. The maximum value of C_N occurs at an angle of attack of 45 degrees for all flow conditions. The maximum value of C_Y varies between 35 and 45 degrees angle of attack, depending on the particular flow condition.
4. Increasing Mach number decreases the magnitude of C_Y . Increasing Reynolds number increases the magnitude of C_Y .
5. The effect of Mach and Reynolds numbers on the magnitude of C_N depends on the particular flow condition.

No general trends were established.

6. Values of C_Y and C_N obtained from the digital computer program do not accurately predict the values of C_N and C_Y obtained experimentally.

7. The theoretical program fails to correctly account for the increase in the magnitude of C_Y with increasing Reynolds number and the decrease in the magnitude of C_Y with increasing Mach number.

8. The theoretical program correctly simulates the general effect of Mach and Reynolds numbers on C_N in comparison with the effects determined experimentally.

9. Flow separation occurs between the 85 and 95 degree points of the cylinder over its entire length for all flow conditions in the nose with grit configuration.

Recommendations

Since a missile designer must be able to predict the aerodynamic forces and moments on a missile given a particular geometry and flight envelope, an adequate prediction technique must be made available to him. To reach this goal, a better understanding of the parameters that affect the induced side forces on a slender body is required. It is therefore necessary to understand the actual vortex shedding phenomena and be able to determine the influence of the shed vortices on the local pressure distributions. In order to accomplish the above, it is recommended that static and pitot pressure measurements be made in the wake of the model in order to determine the spacing, locations, and strengths of the shed

vortices. The results should provide a better physical model of the flow field and therefore better input constants to the multi-vortex model prediction program.

VII. Figures

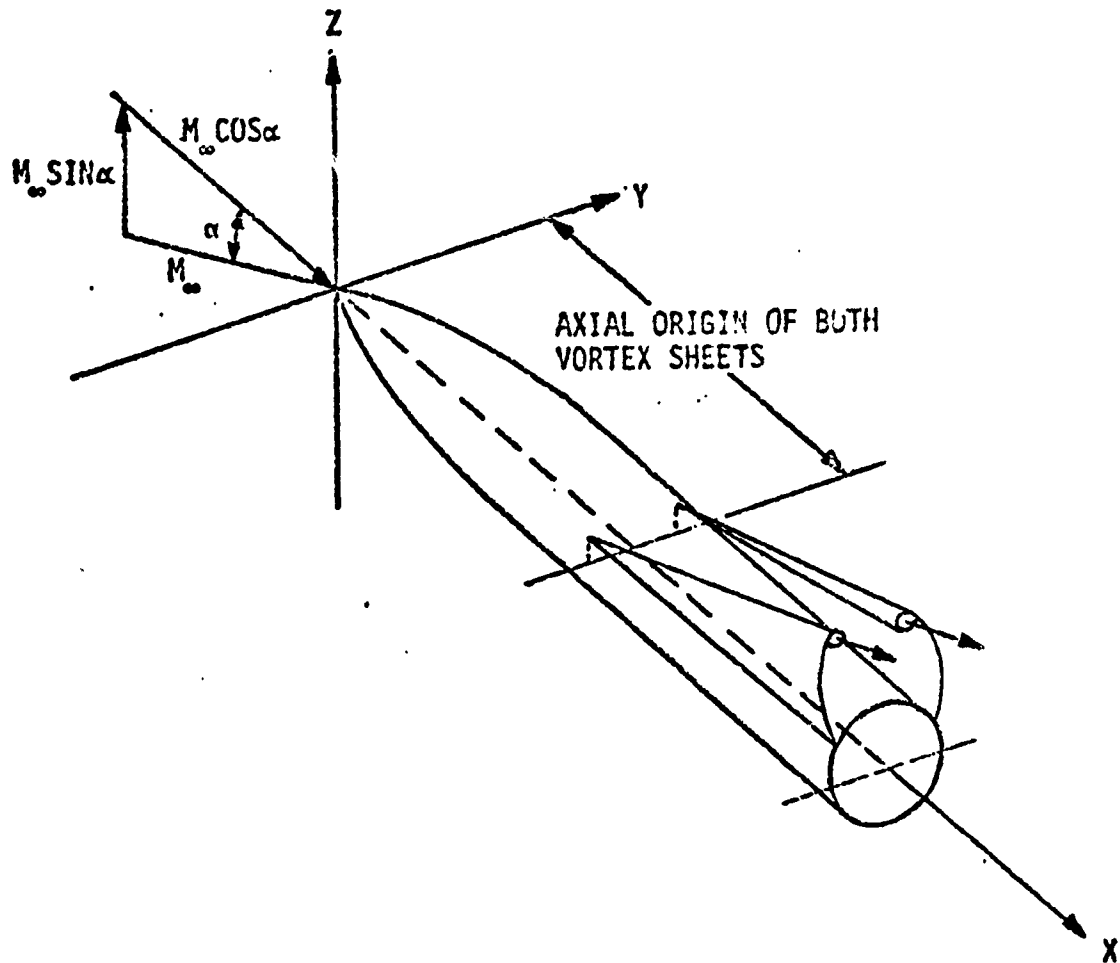
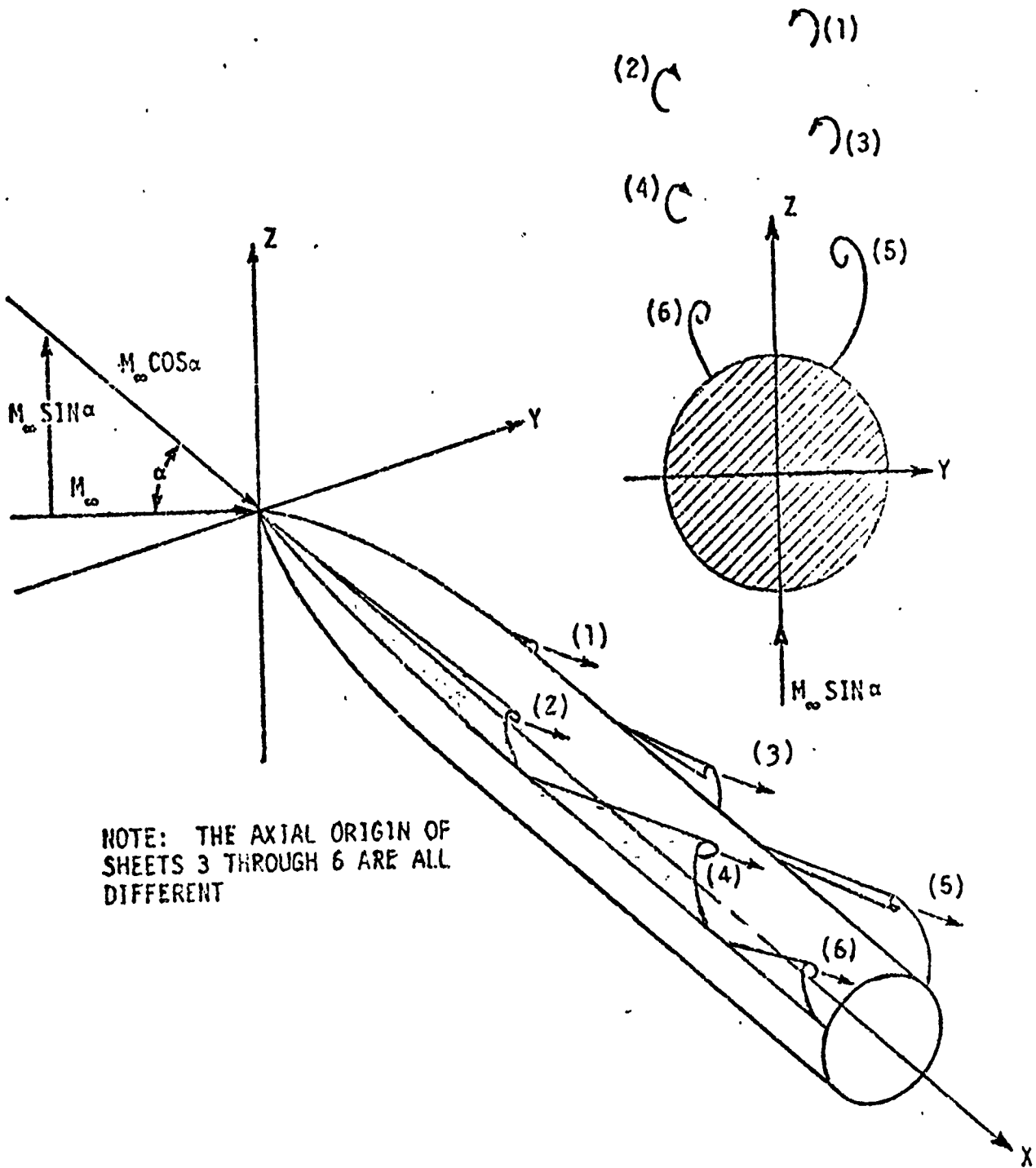


Fig 1. Steady, Symmetric Vortices ($5^\circ < \alpha < 25^\circ$) (Ref 2)



NOTE: THE AXIAL ORIGIN OF SHEETS 3 THROUGH 6 ARE ALL DIFFERENT

Fig 2. Steady, Asymmetric Vortices ($25^\circ < \alpha < 50^\circ$) (Ref 2)

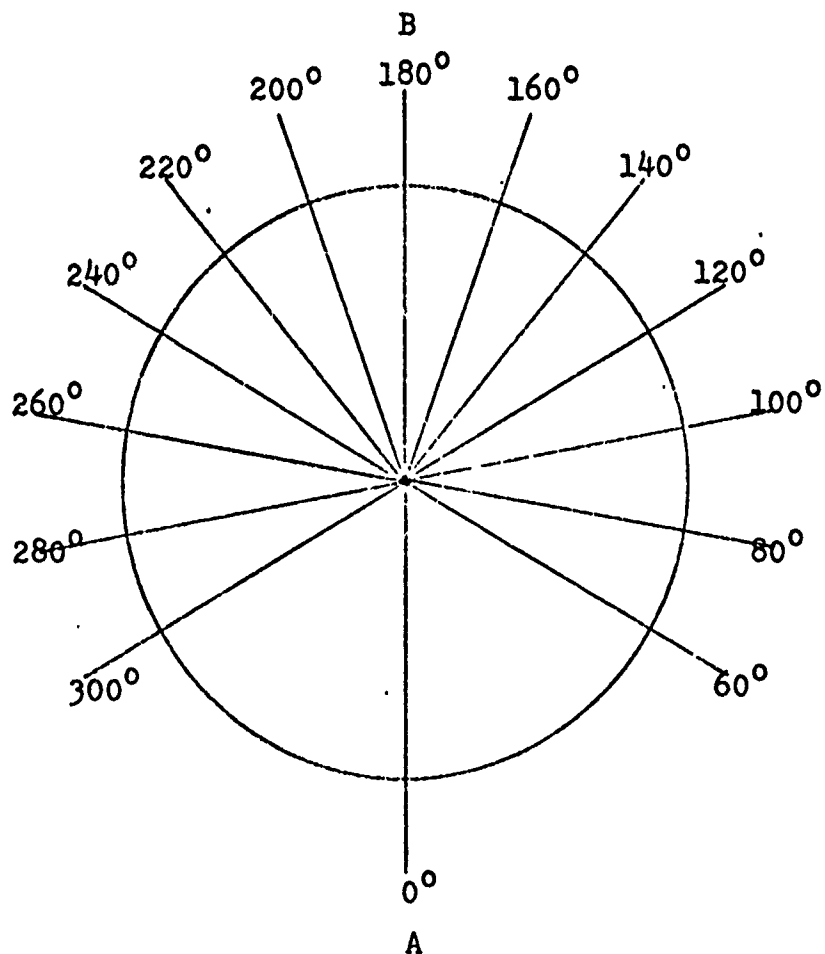
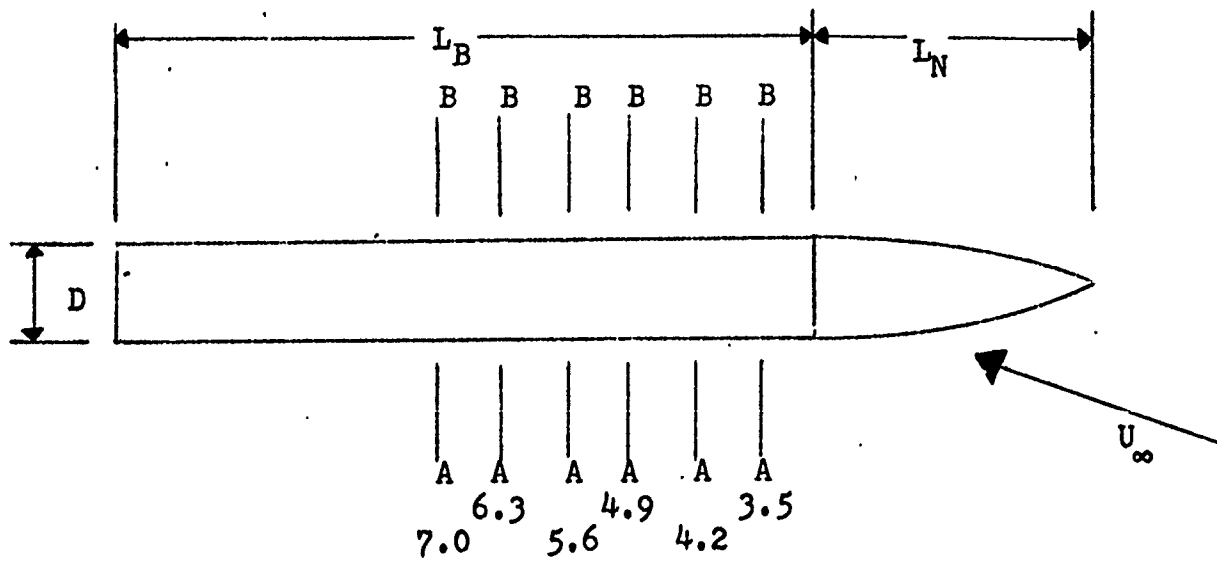


Fig 3. Model Pressure Orifice Location

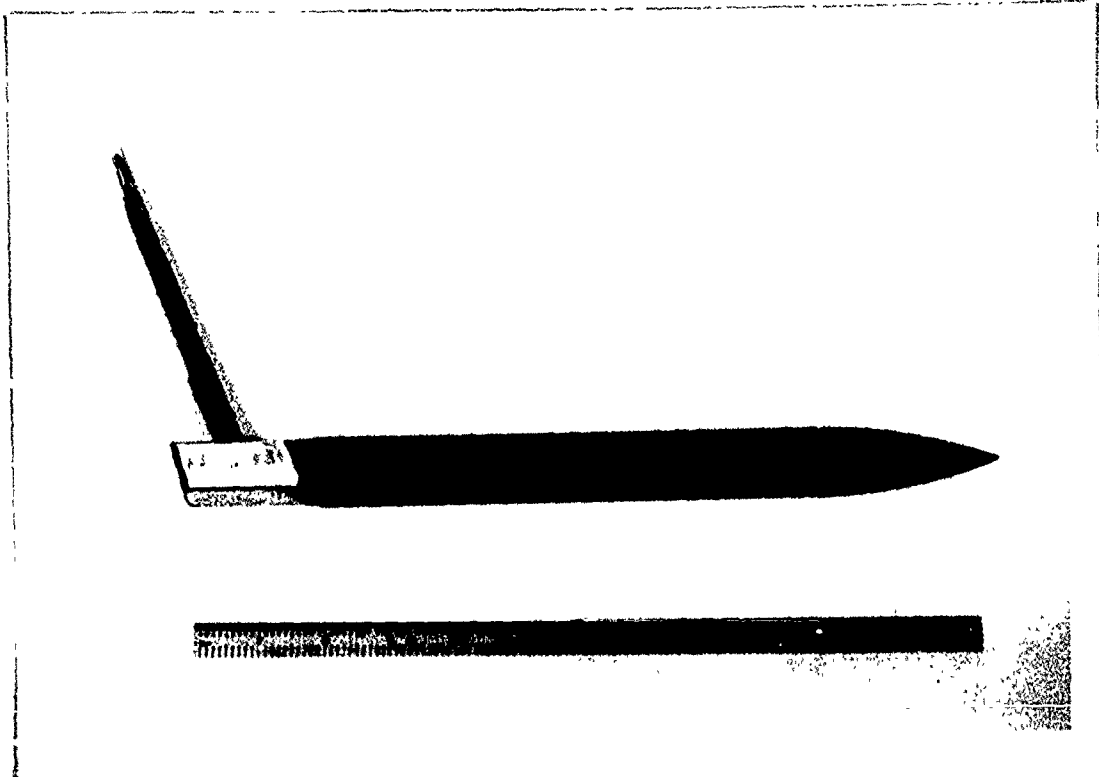


Fig 4. Axisymmetric Model Tested



Fig 5. Model and Support Section



Fig 6. Model and Support Section Installed In TGF

$RE = 1.0 \times 10^6 / FT$
 $MACH = .3$
 $X/D = 5.6$

□ ALPHA = 27
 ○ ALPHA = 30
 ▲ ALPHA = 35
 + ALPHA = 40
 X ALPHA = 45

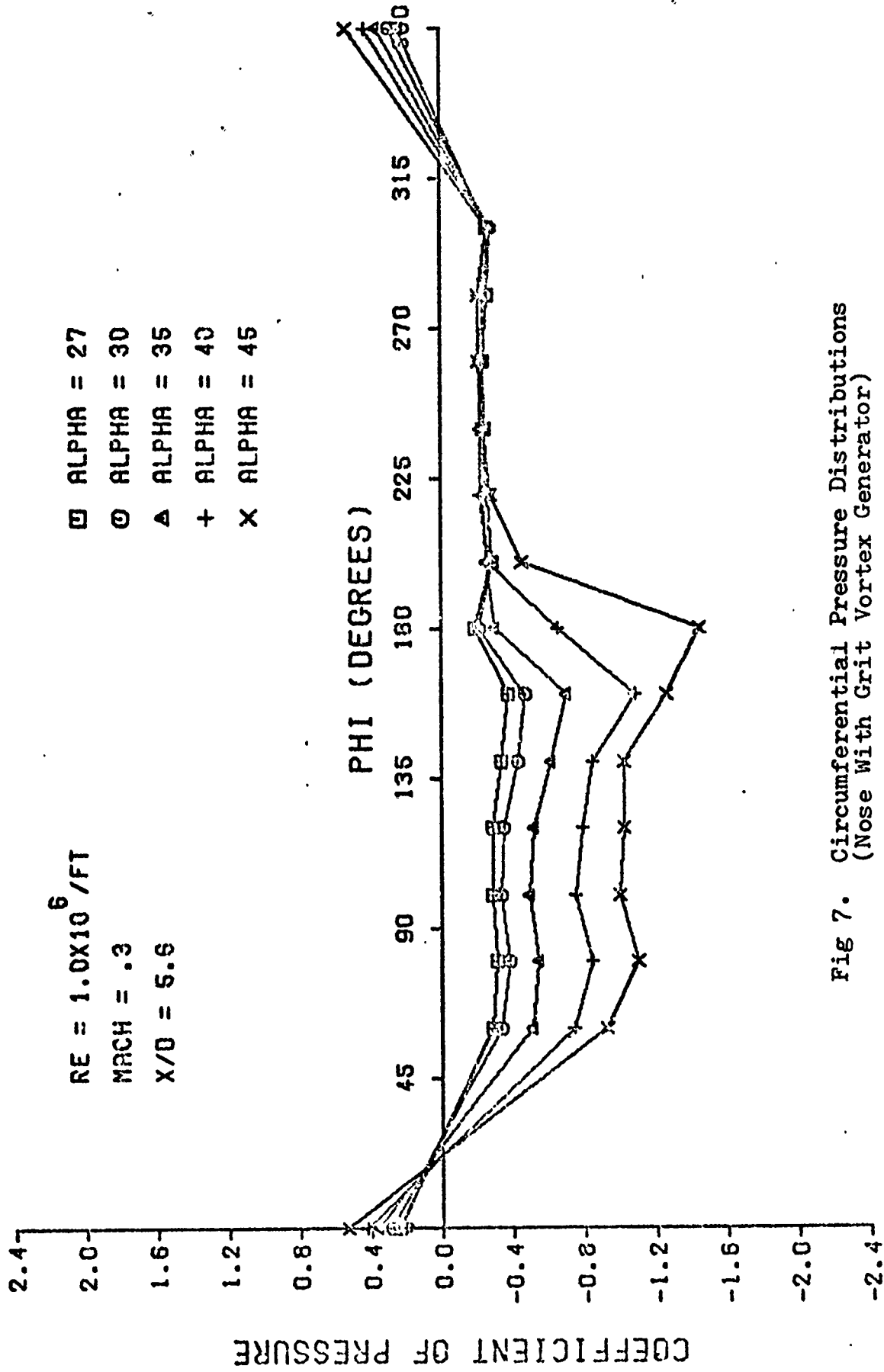


Fig 7. Circumferential Pressure Distributions (Nose With Grit Vortex Generator)

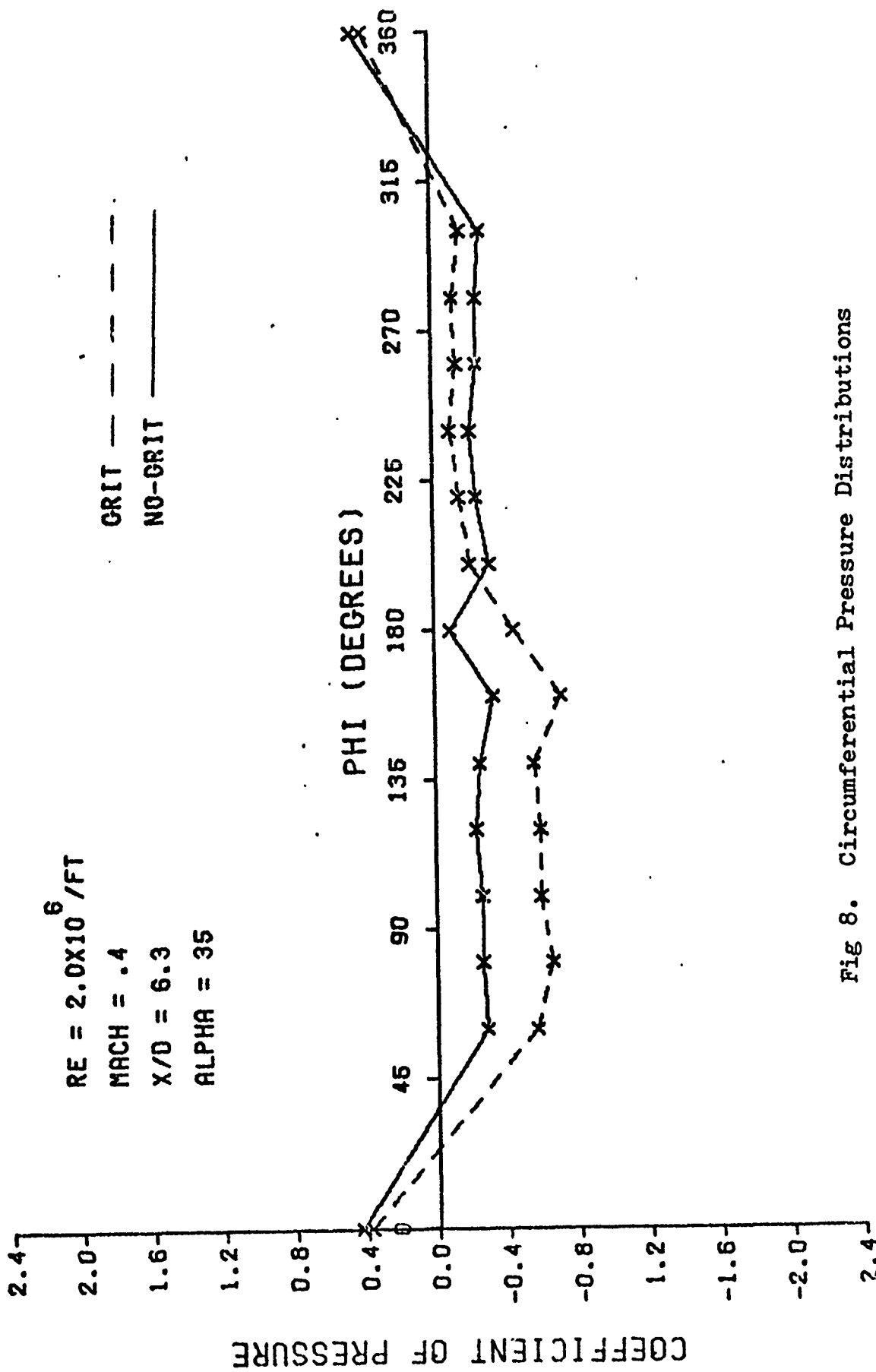


Fig 8. Circumferential Pressure Distributions

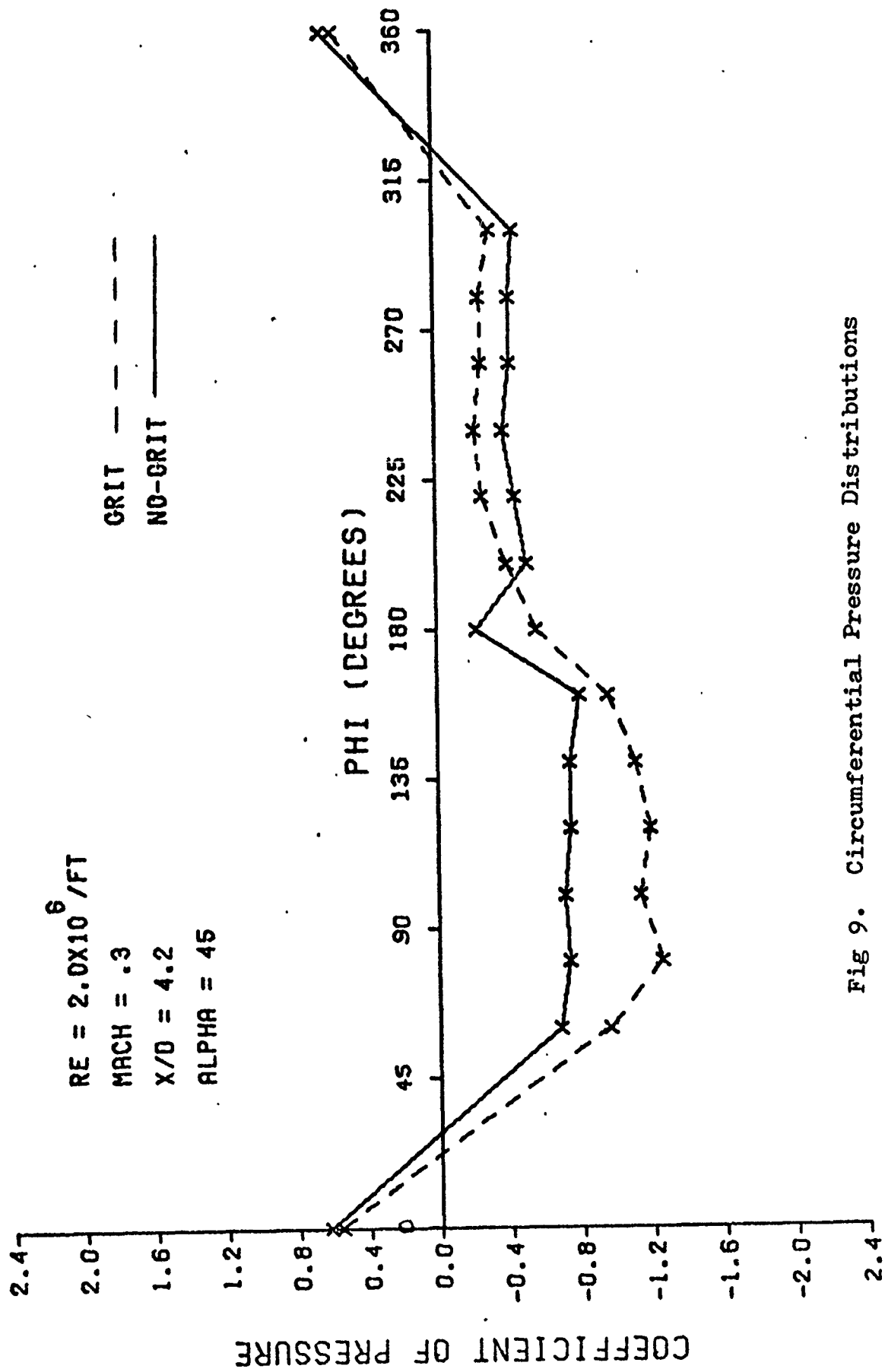


Fig 9. Circumferential Pressure Distributions

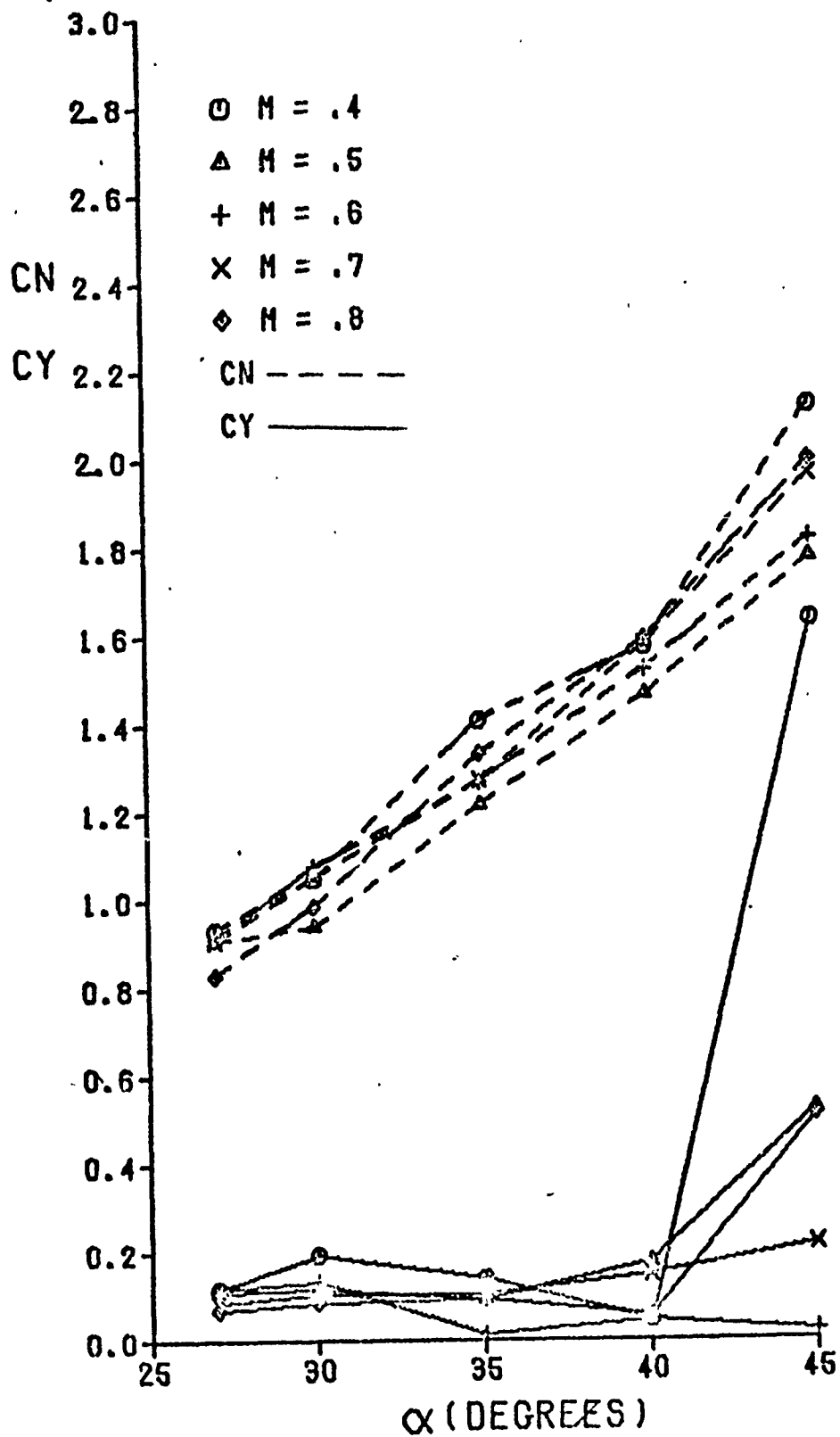


Fig 10. Effect of Mach Number on Local Side and Normal Force Coefficients at $Re_D = 41,667$

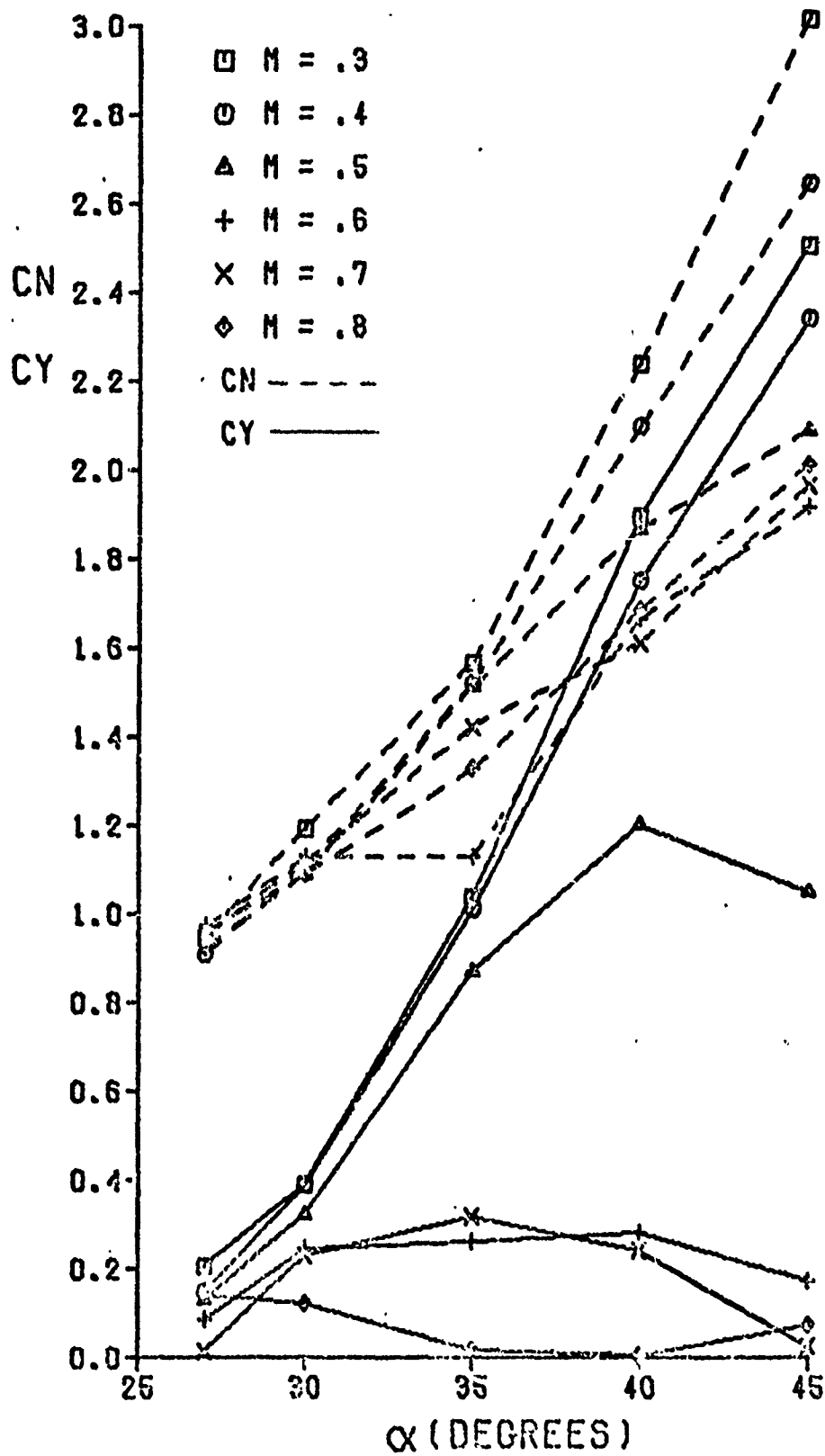


Fig 11. Effect of Mach Number on Local Side and Normal Force Coefficients at $Re_D = 83,333$

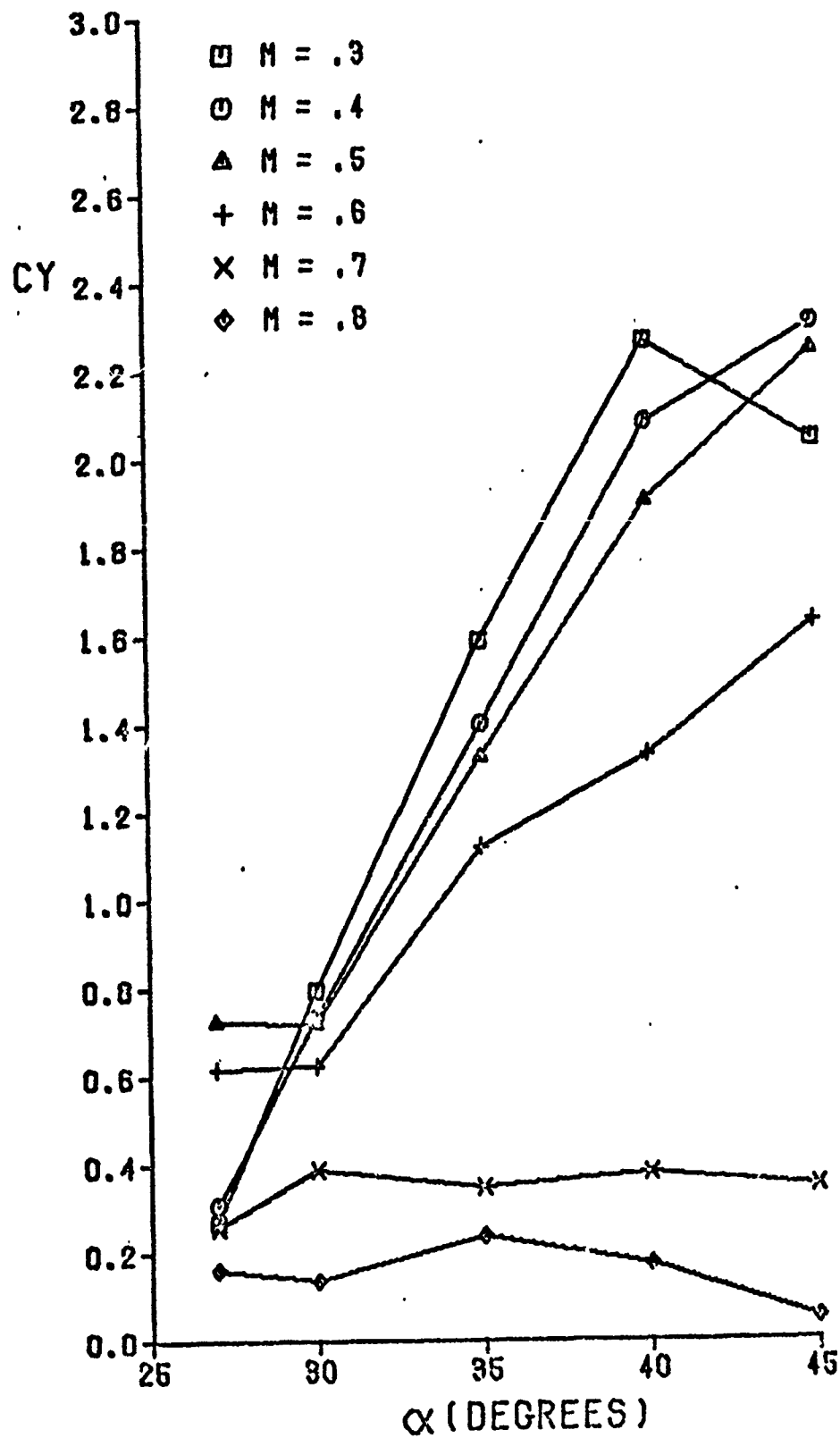


Fig 12. Effect of Mach Number on Local Side Force Coefficient at $Re_D = 166,667$

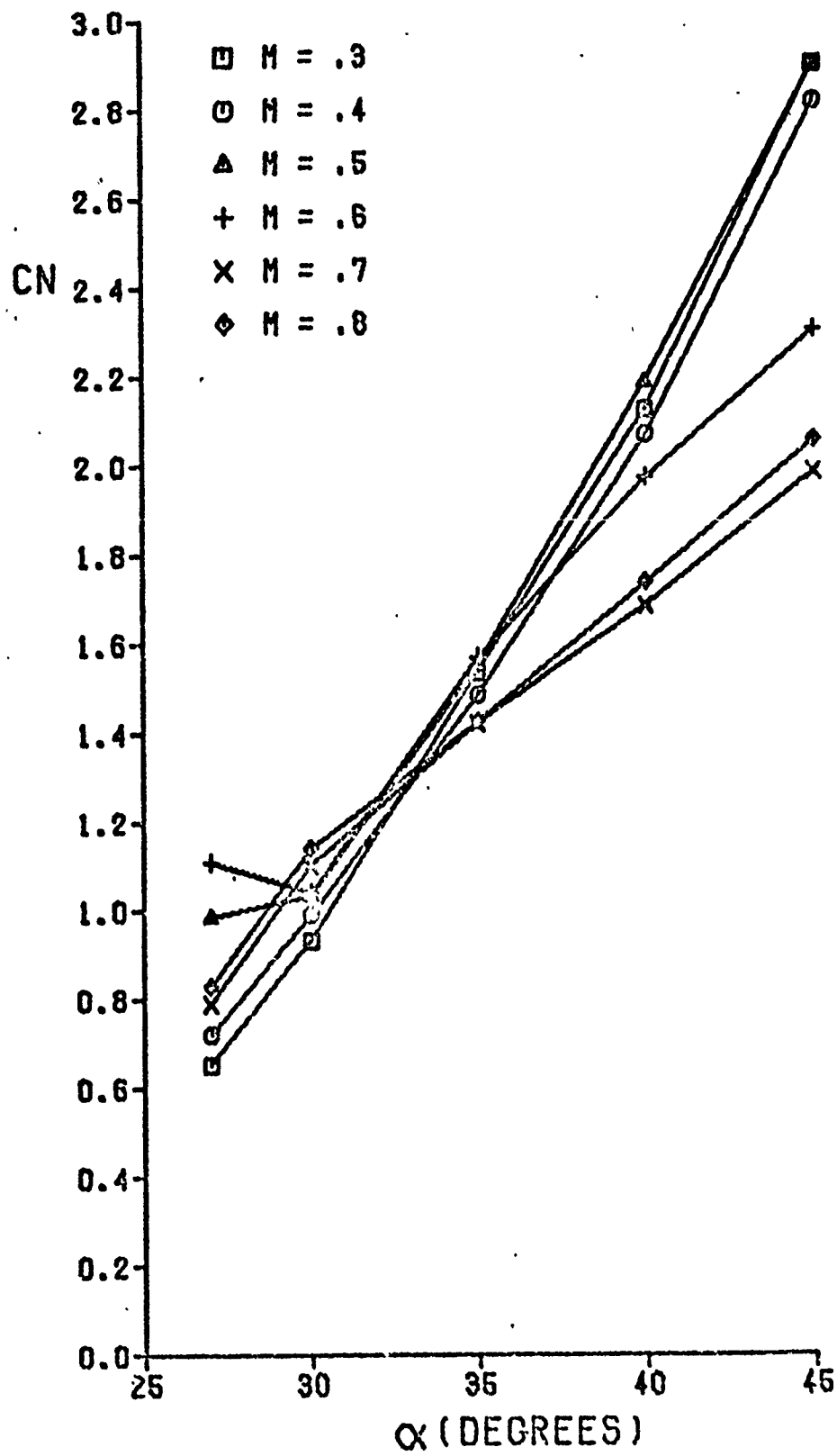


Fig 13. Effect of Mach Number on Local Normal Force Coefficient at $Re_D = 166,667$

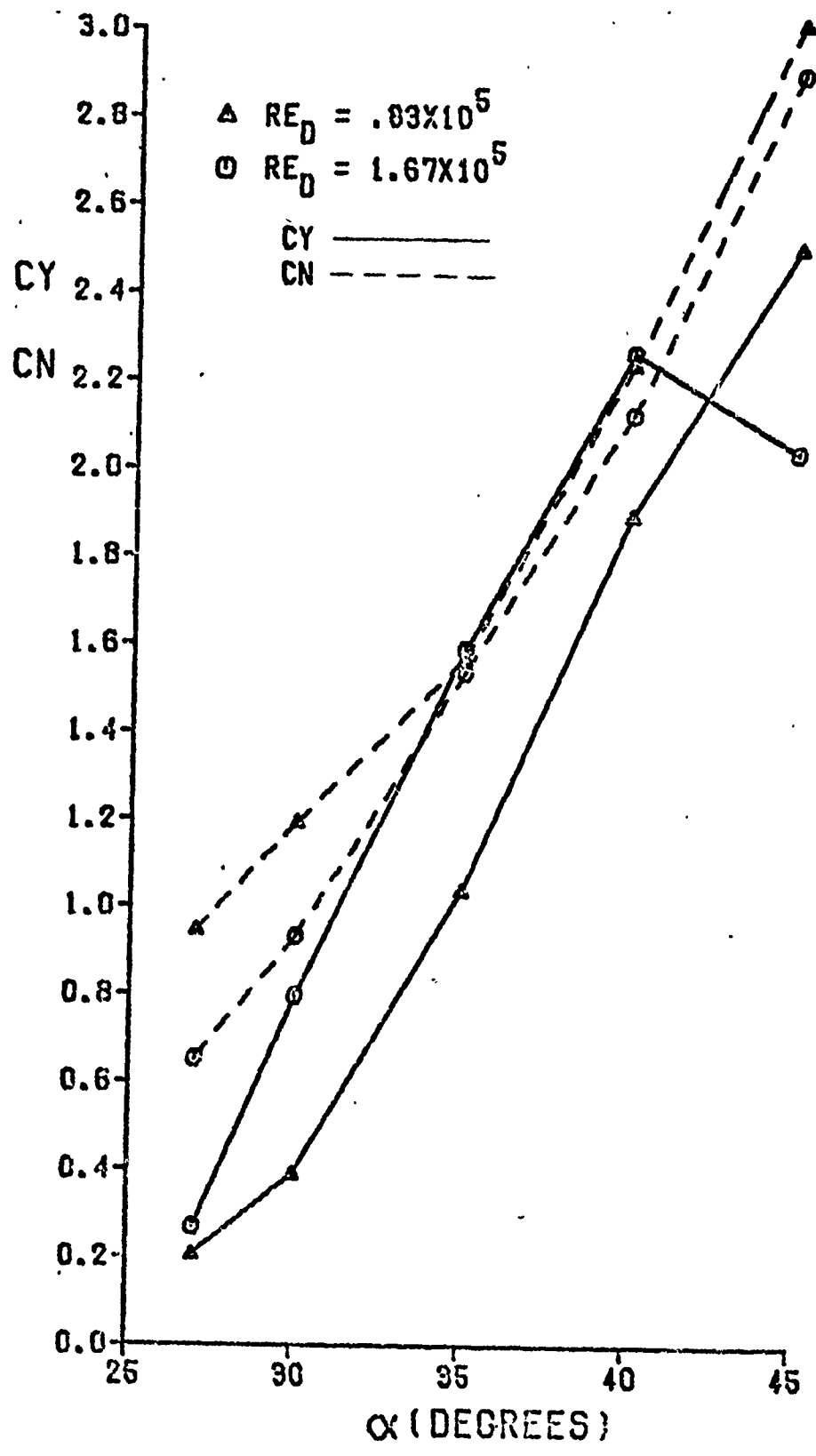


Fig 14. Effect of Reynolds Number on Local Side and Normal Force Coefficients at $M = .3$

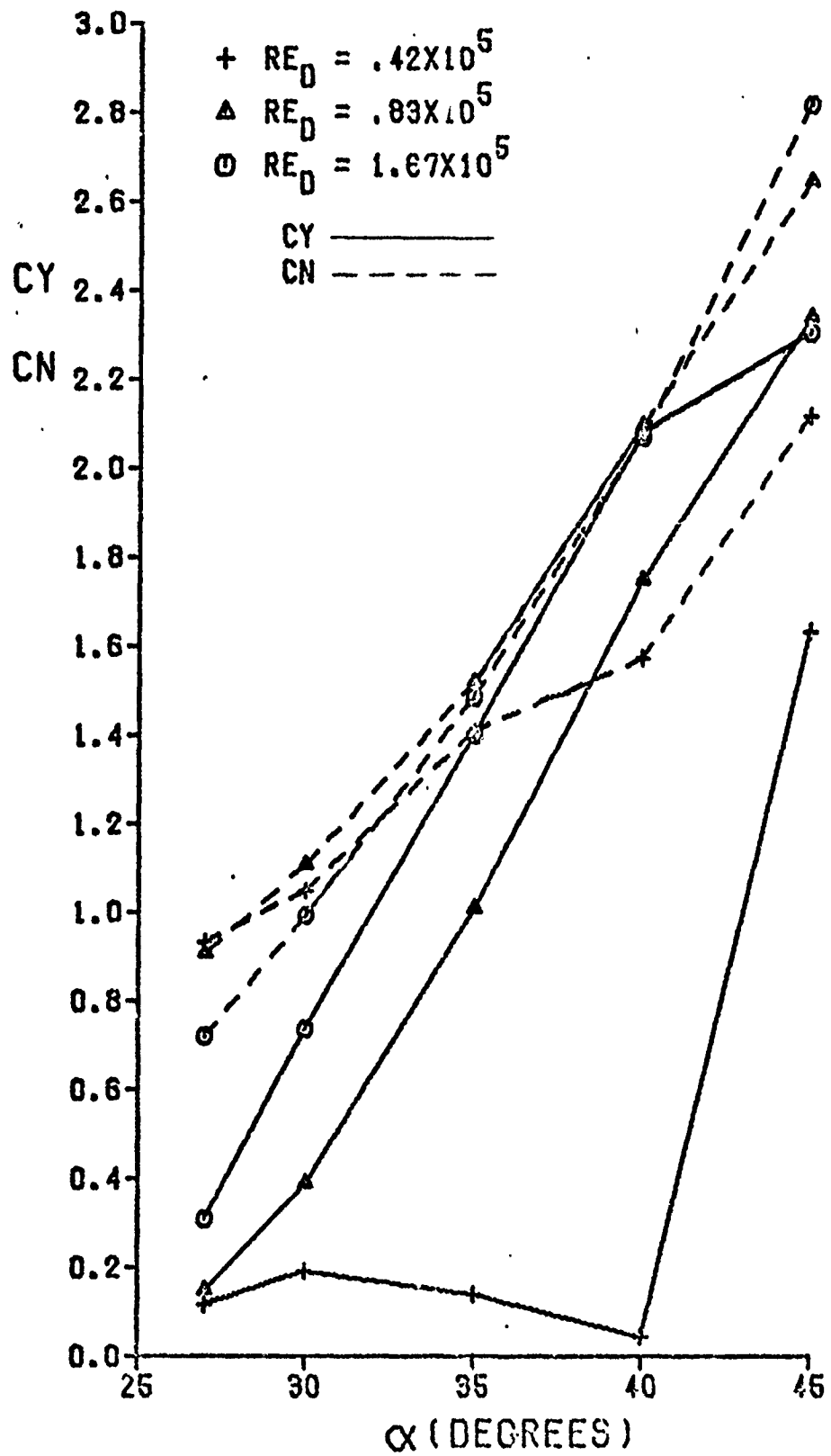


Fig 15. Effect of Reynolds Number on Local Side and Normal Force Coefficients at $M = .4$

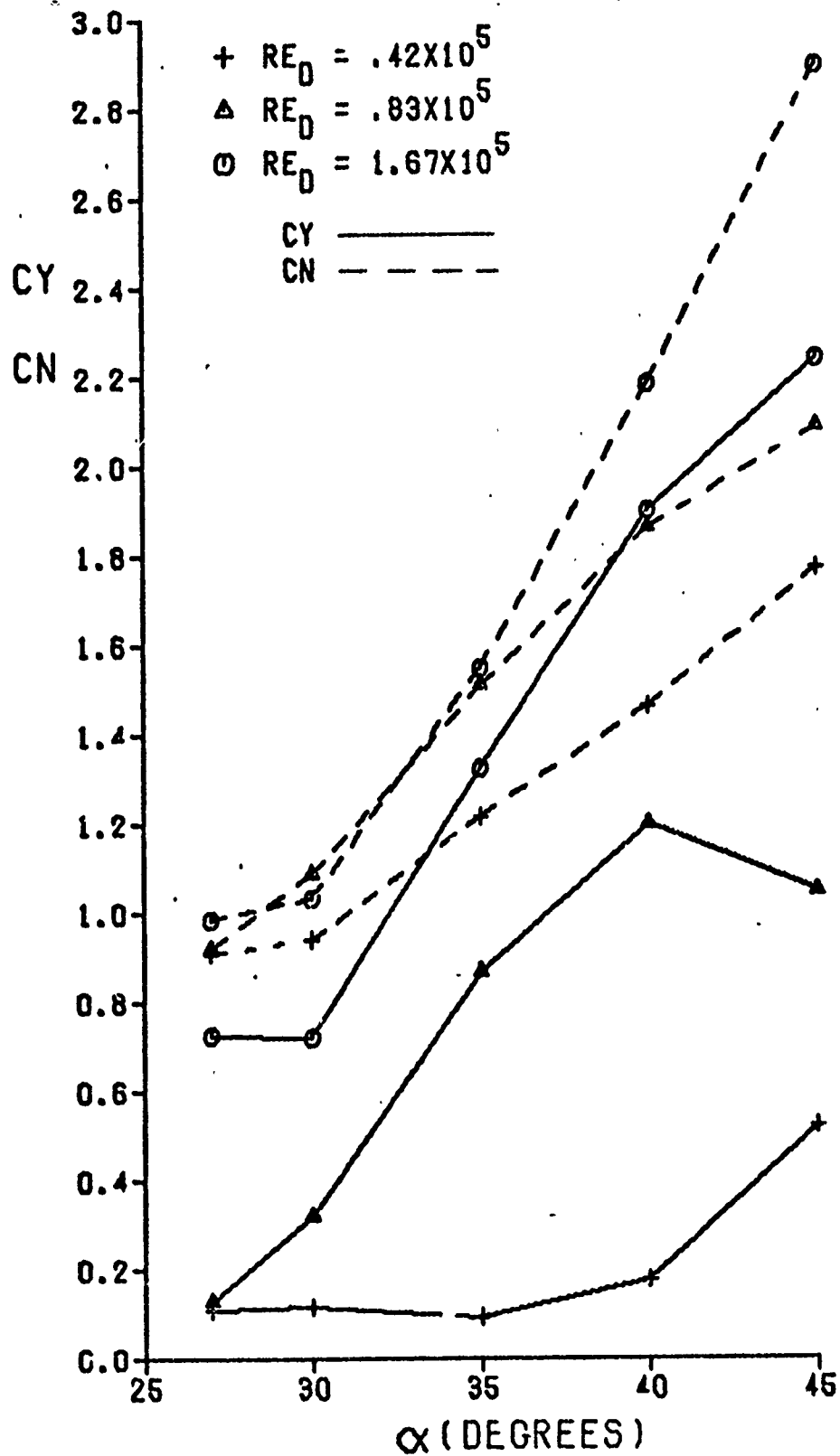


Fig 16. Effect of Reynolds Number on Local Side and Normal Force Coefficients at $M = .5$

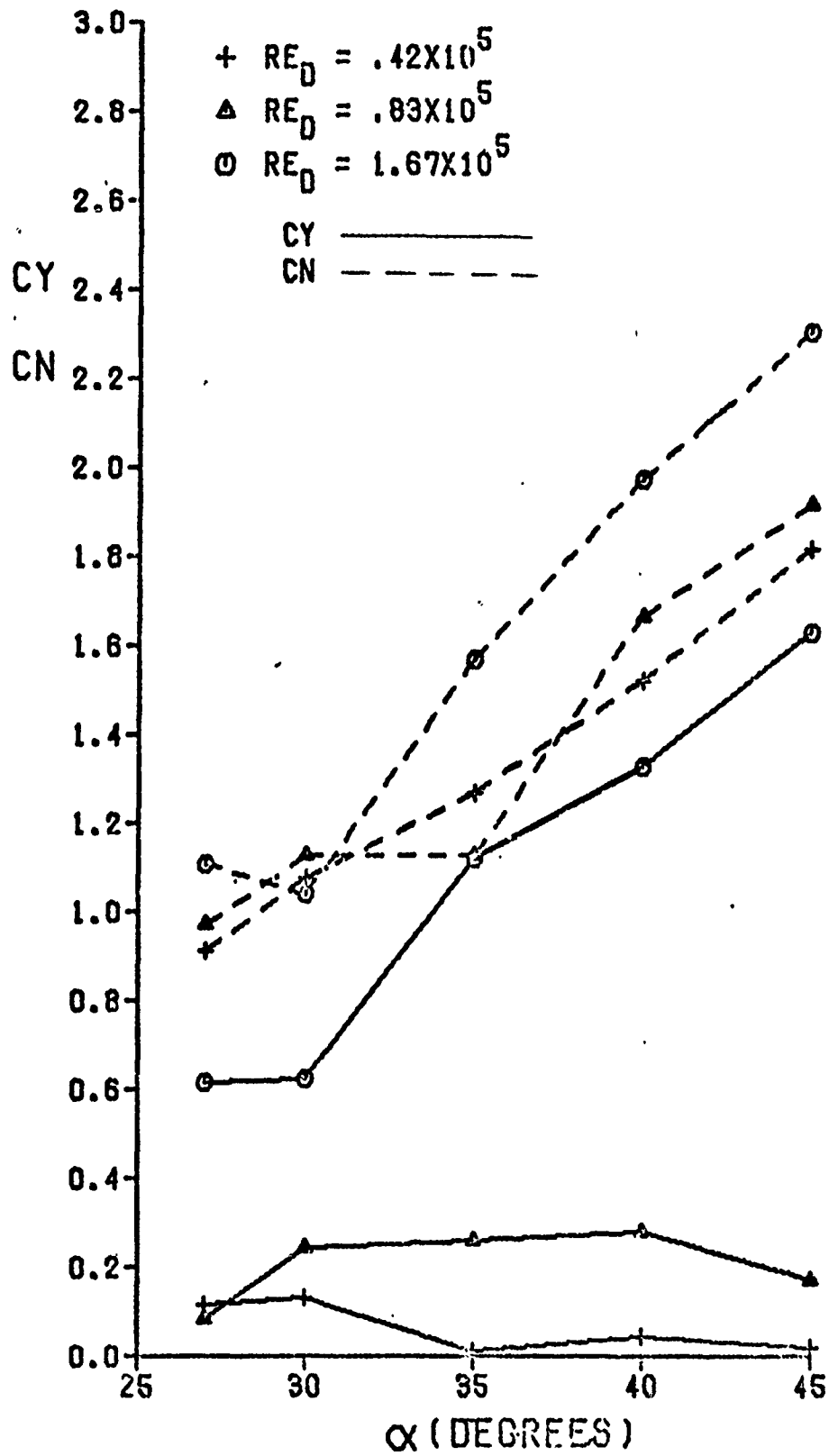


Fig 17. Effect of Reynolds Number on Local Side and Normal Force Coefficients at $M = .6$

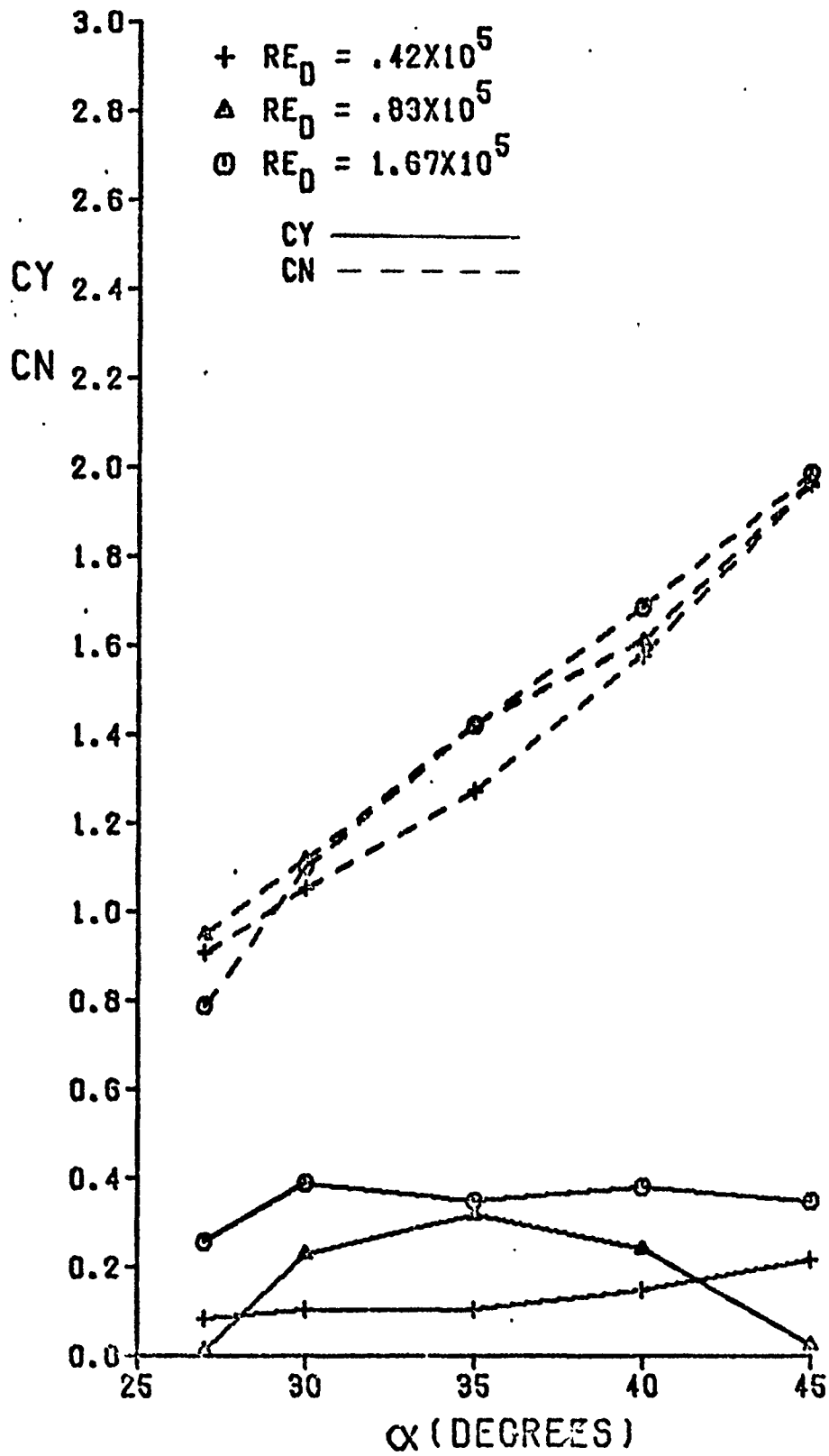


Fig 18. Effect of Reynolds Number on Local Side and Normal Force Coefficients at $M = .7$

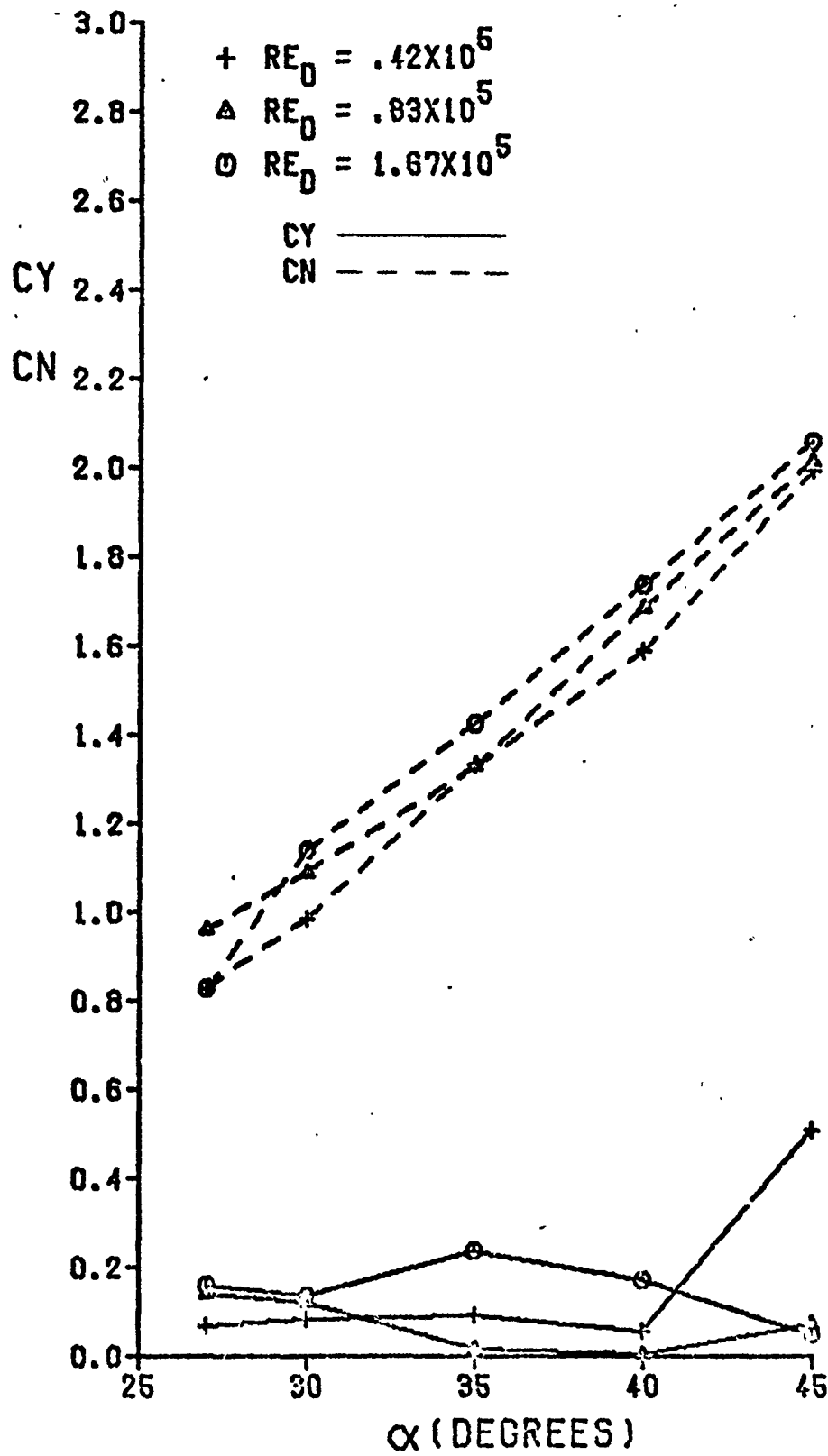


Fig 19. Effect of Reynolds Number on Local Side and Normal Force Coefficients at $M = .8$

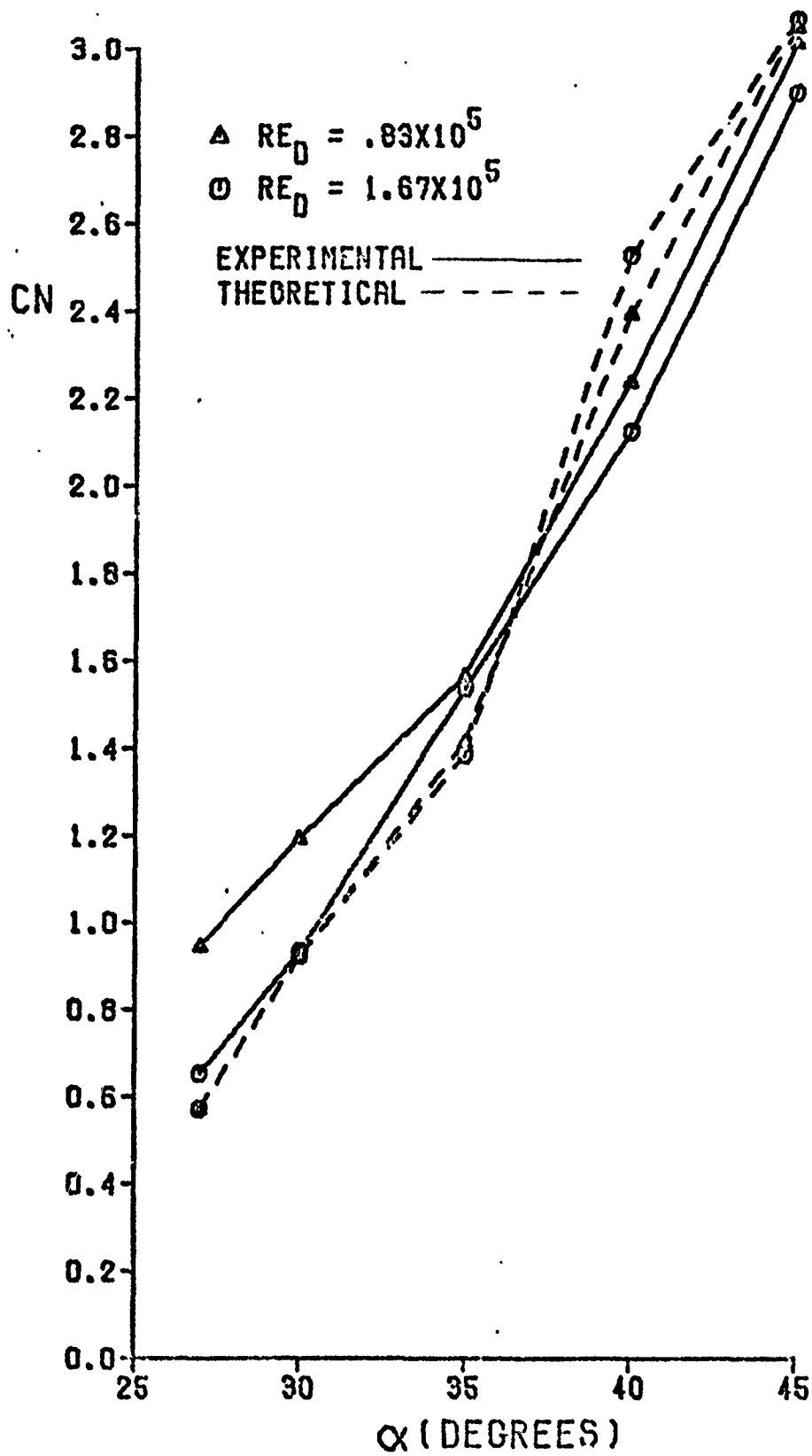


Fig 20. Local Normal Force Coefficient at $M = .3$

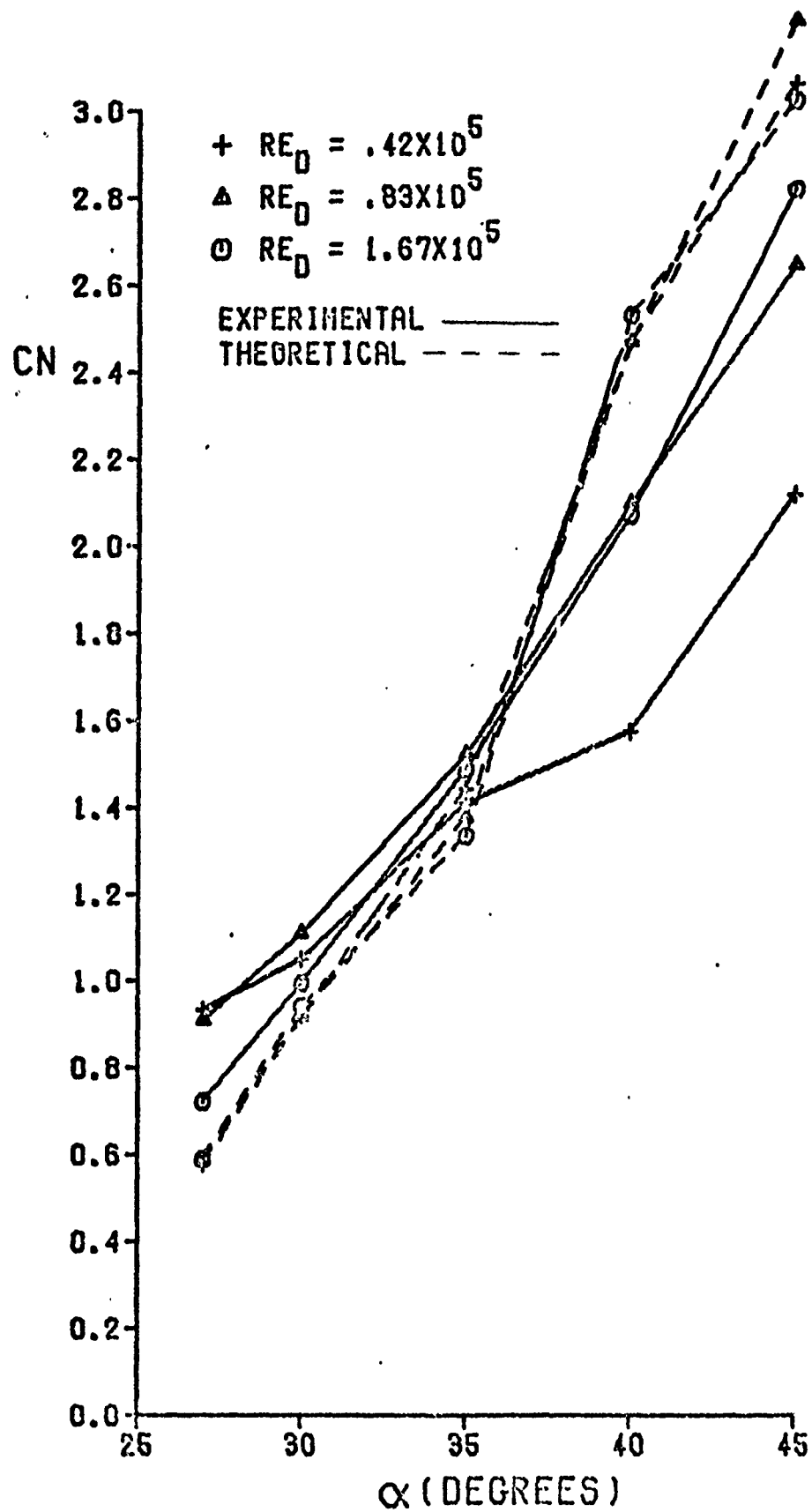


Fig 21. Local Normal Force Coefficient at $M = .4$

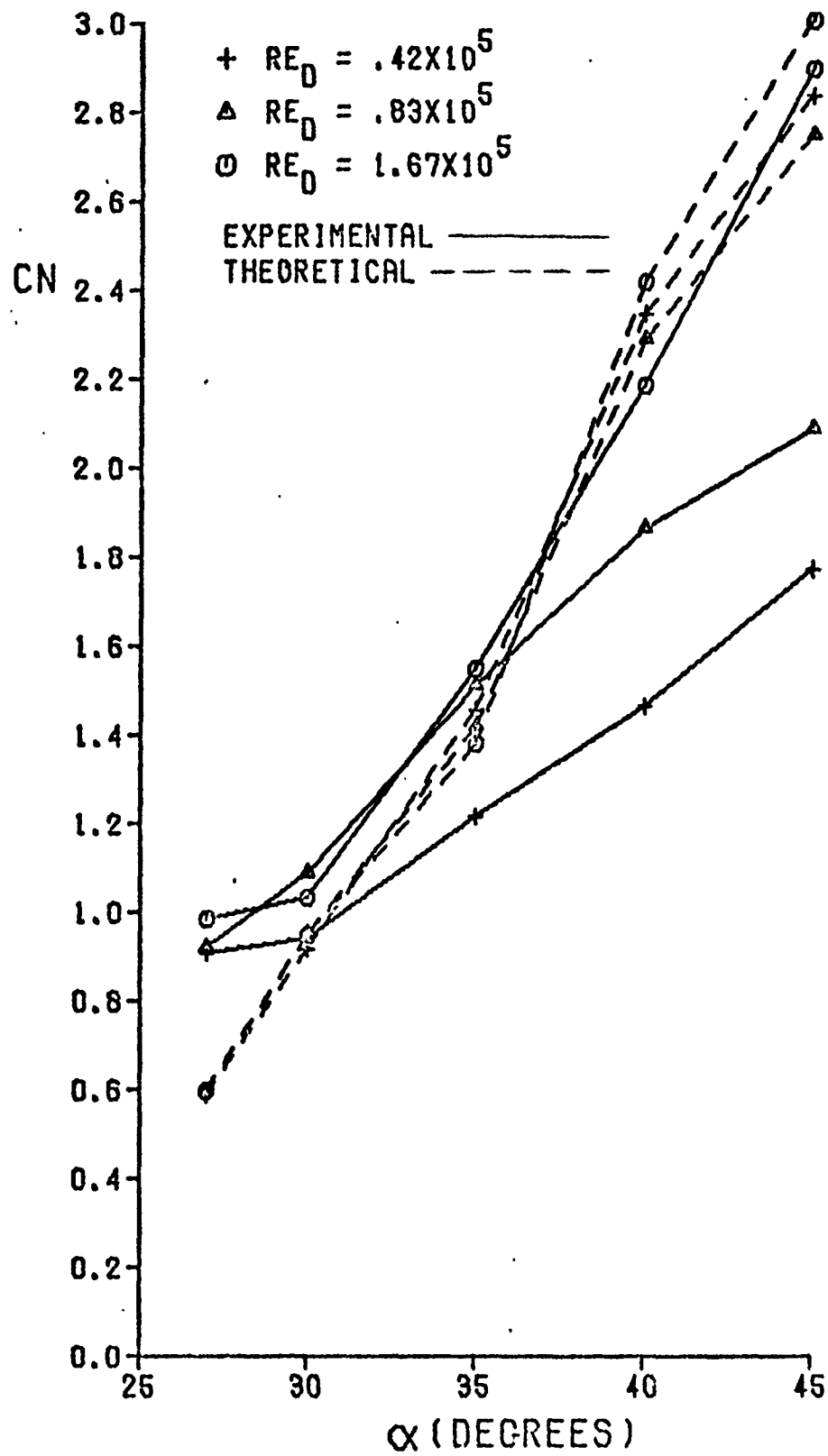


Fig 22. Local Normal Force Coefficient at $M = .5$

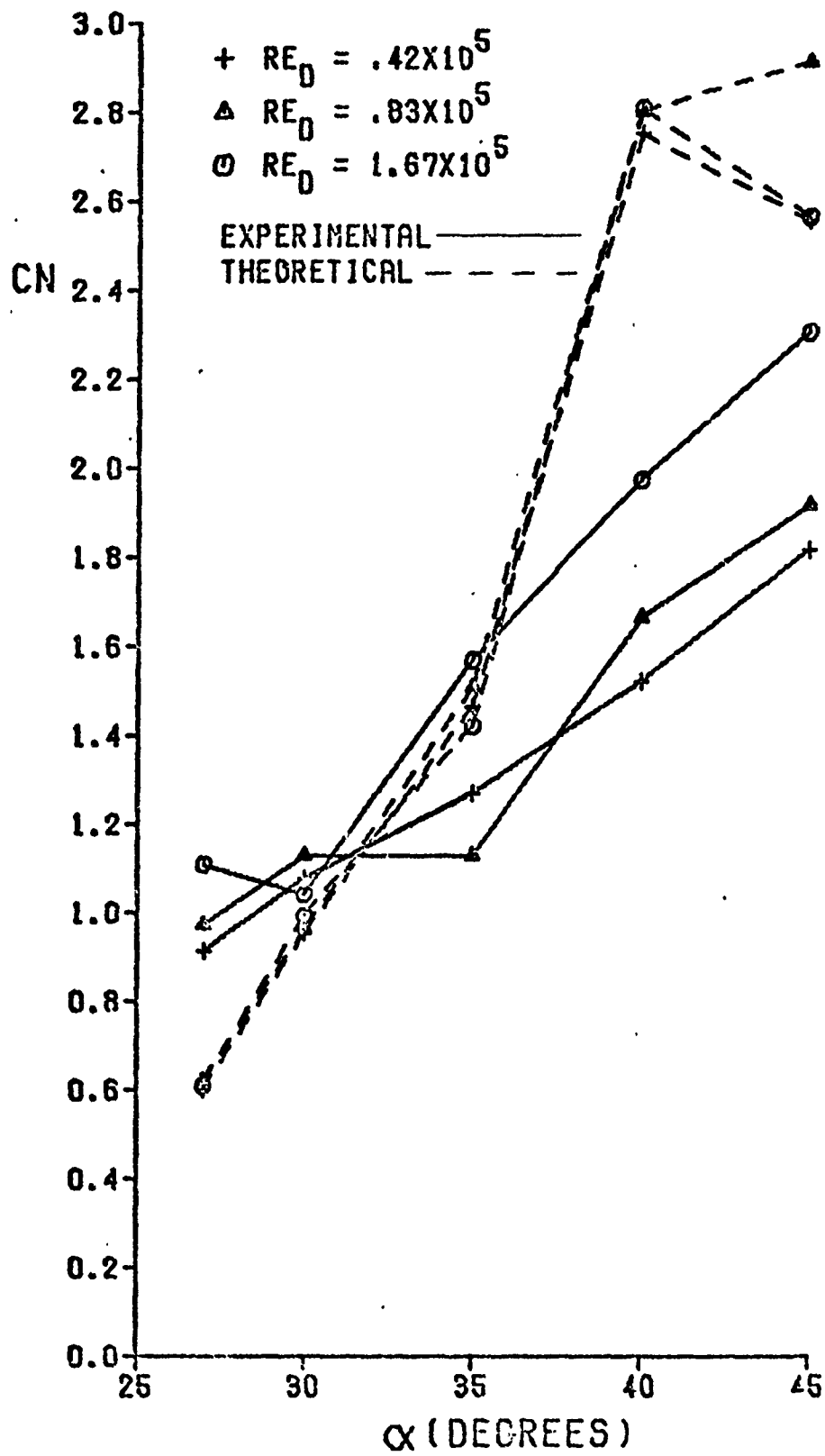


Fig 23. Local Normal Force Coefficient at $M = .6$

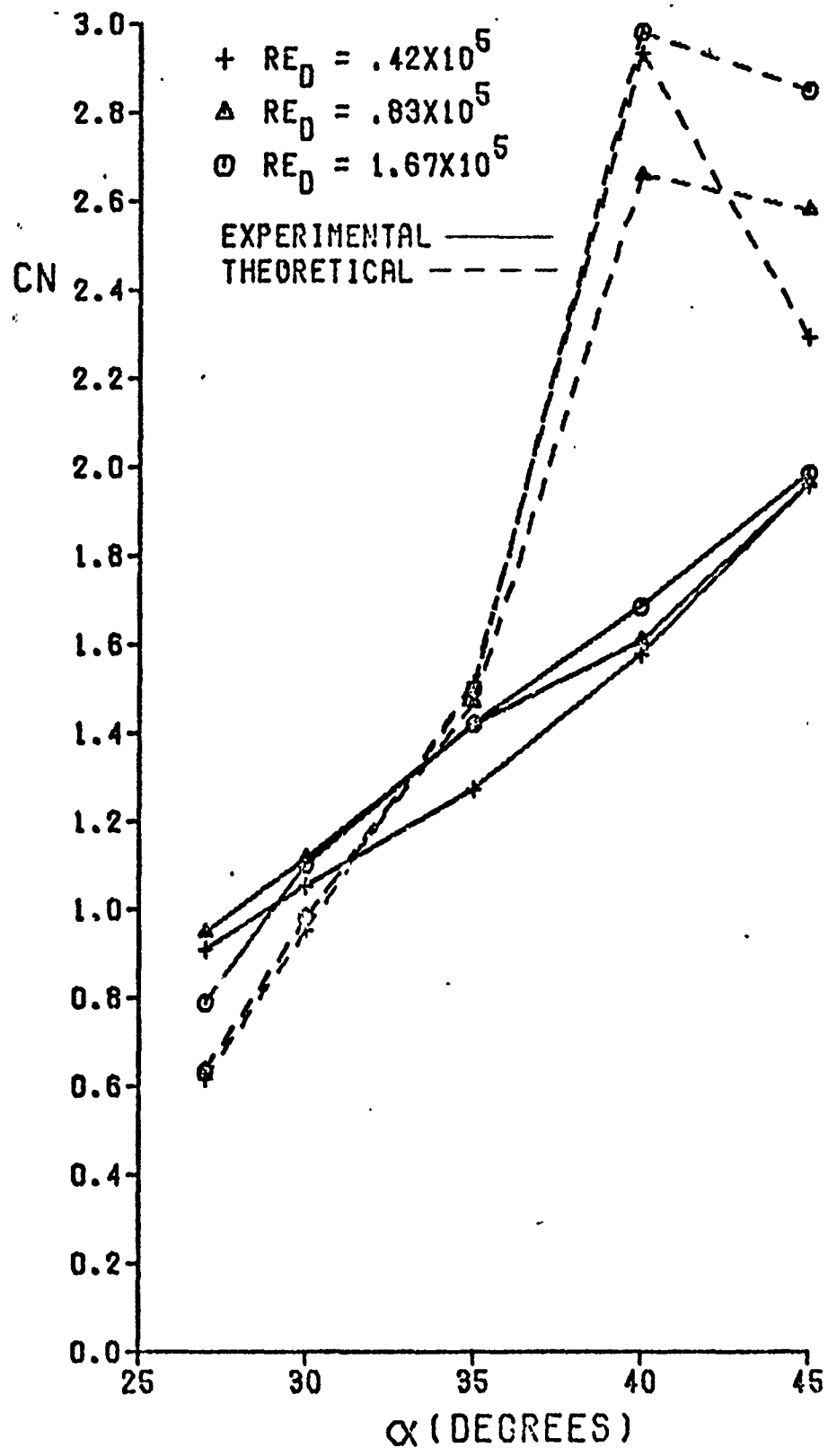


Fig 24. Local Normal Force Coefficient at $M = .7$

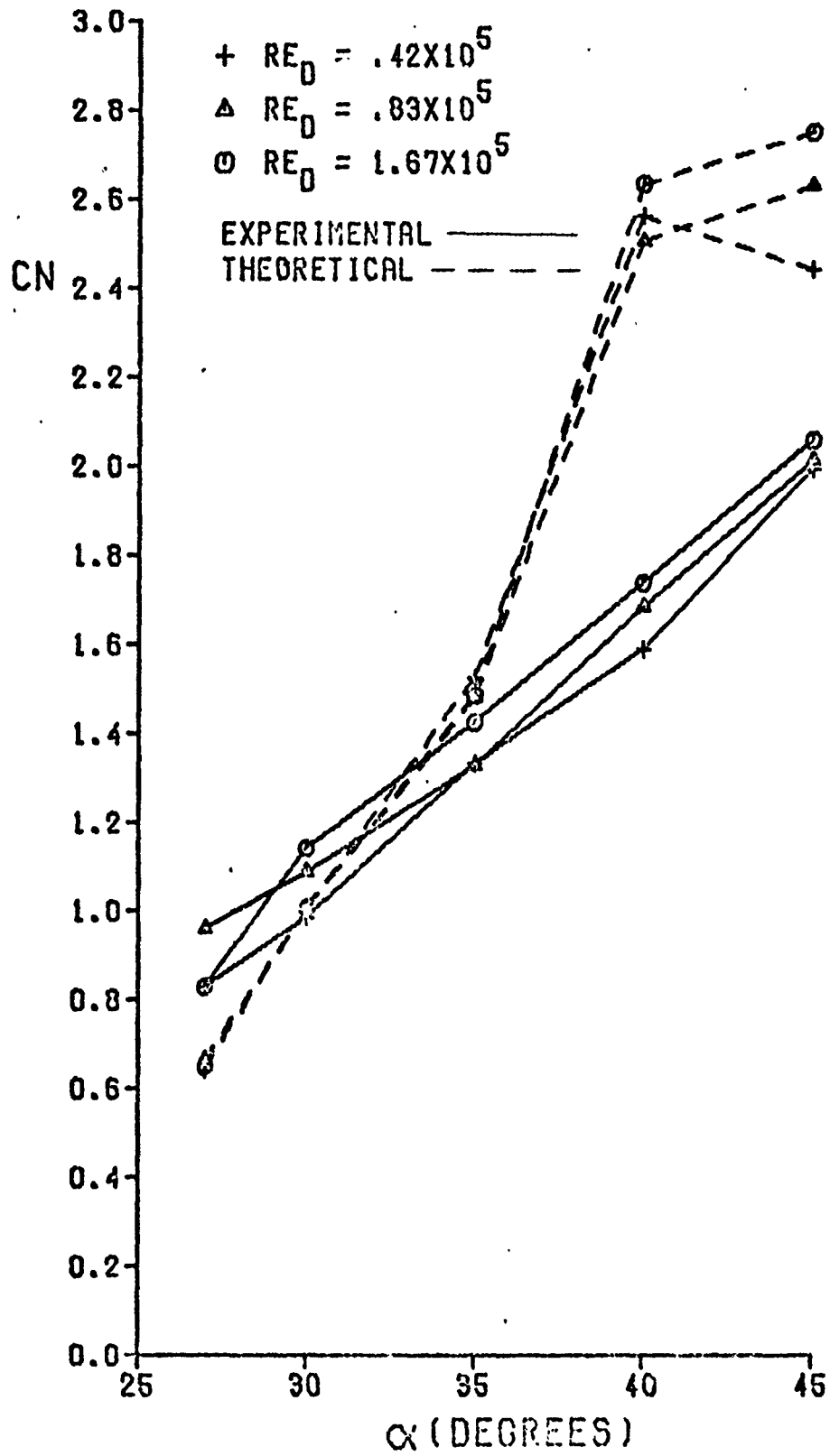


Fig 25. Local Normal Force Coefficient at $M = .8$

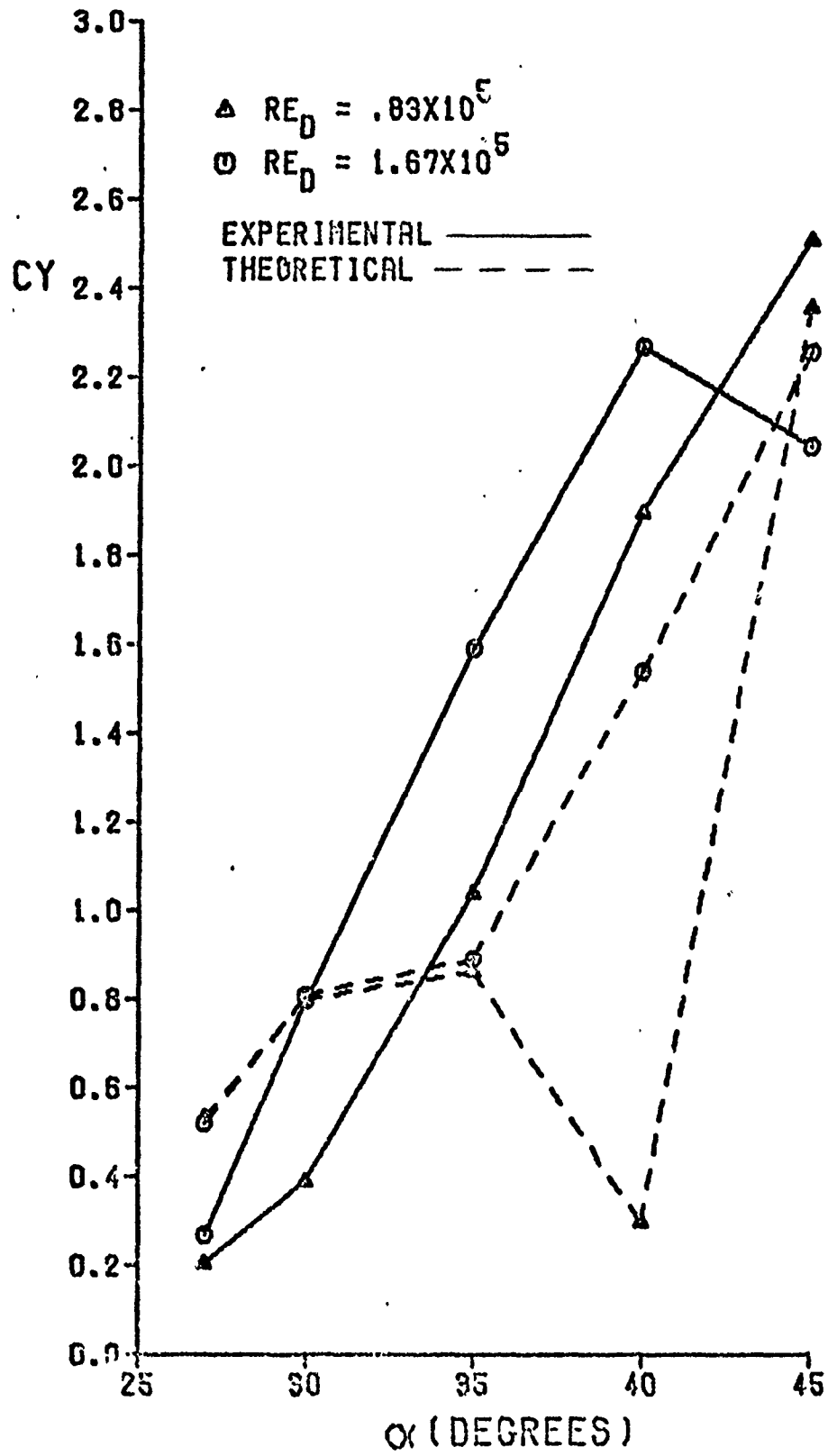


Fig 26. Local Side Force Coefficient at $M = .3$

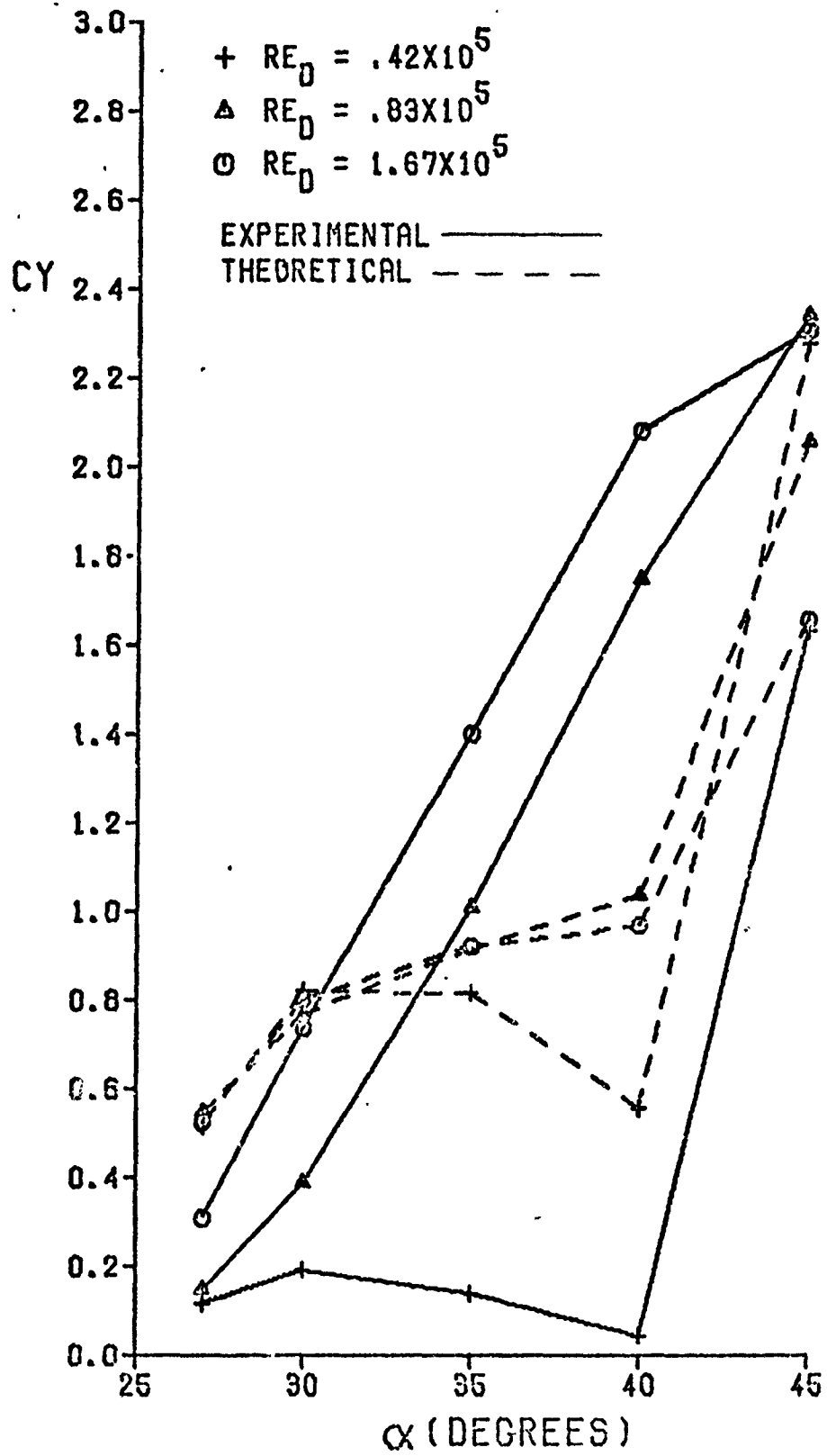


Fig 27. Local Side Force Coefficient at $M = .4$

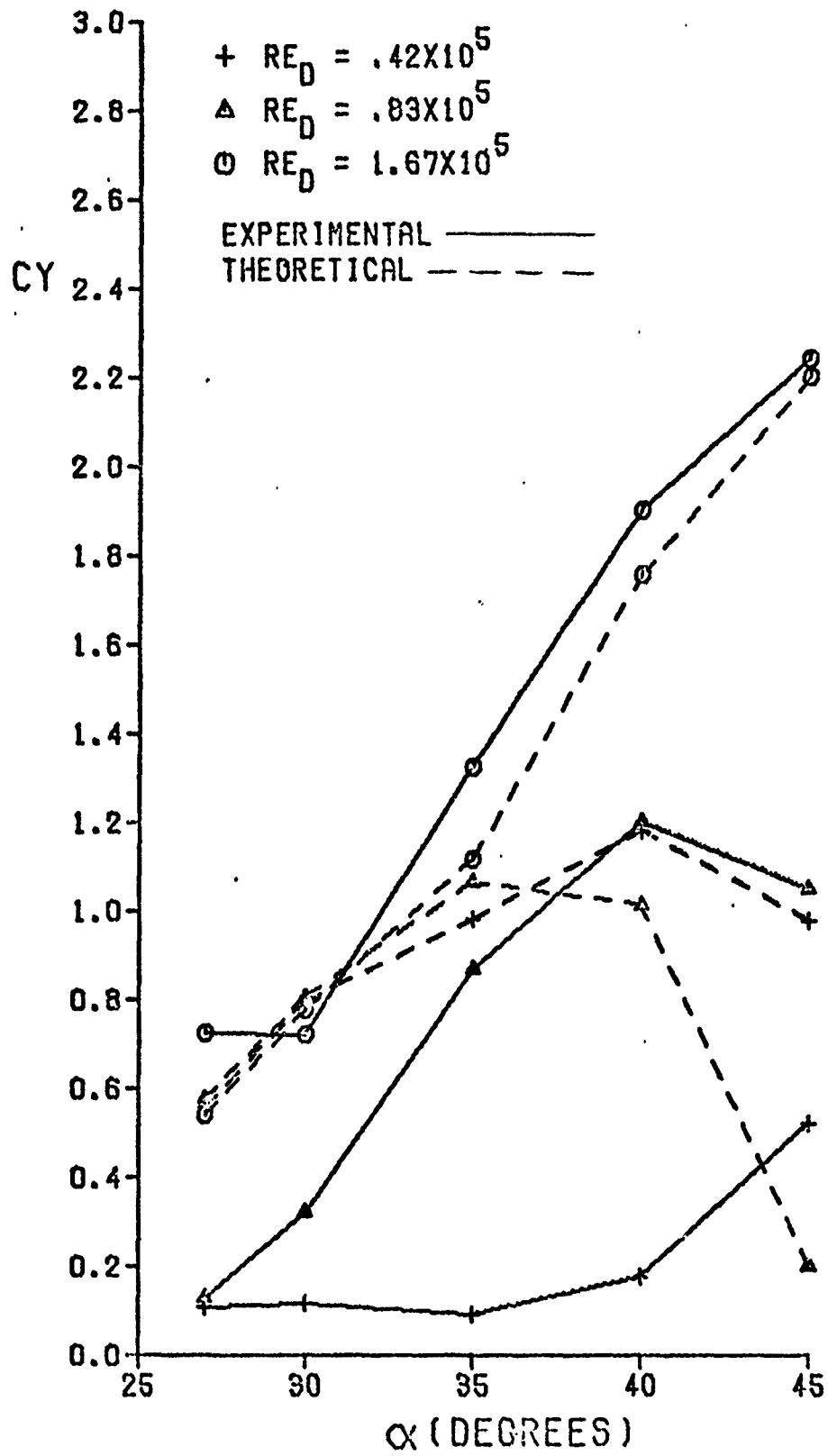


Fig 28. Local Side Force Coefficient at $M = .5$

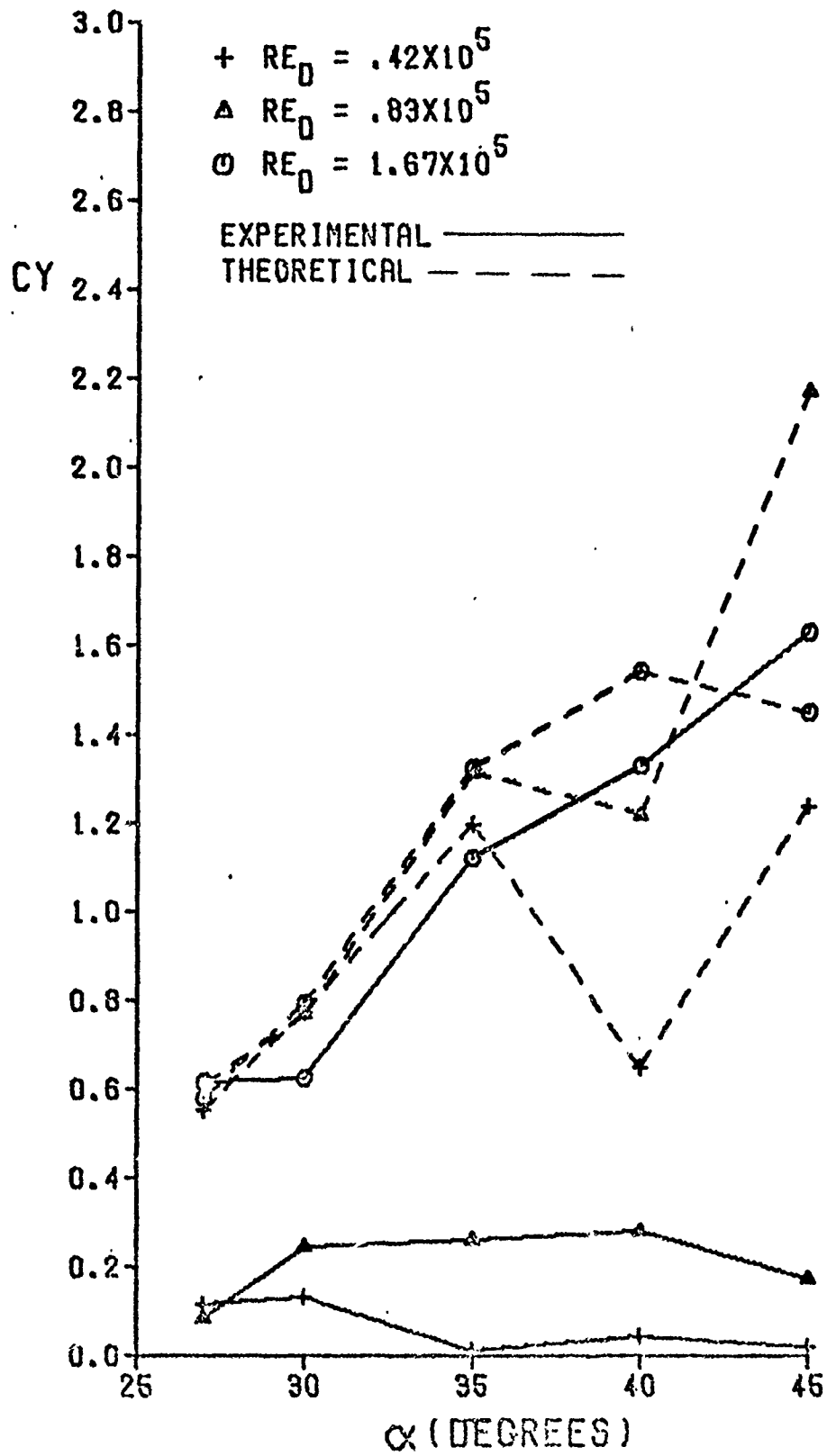


Fig. 29. Local Side Force Coefficient at $M = .6$

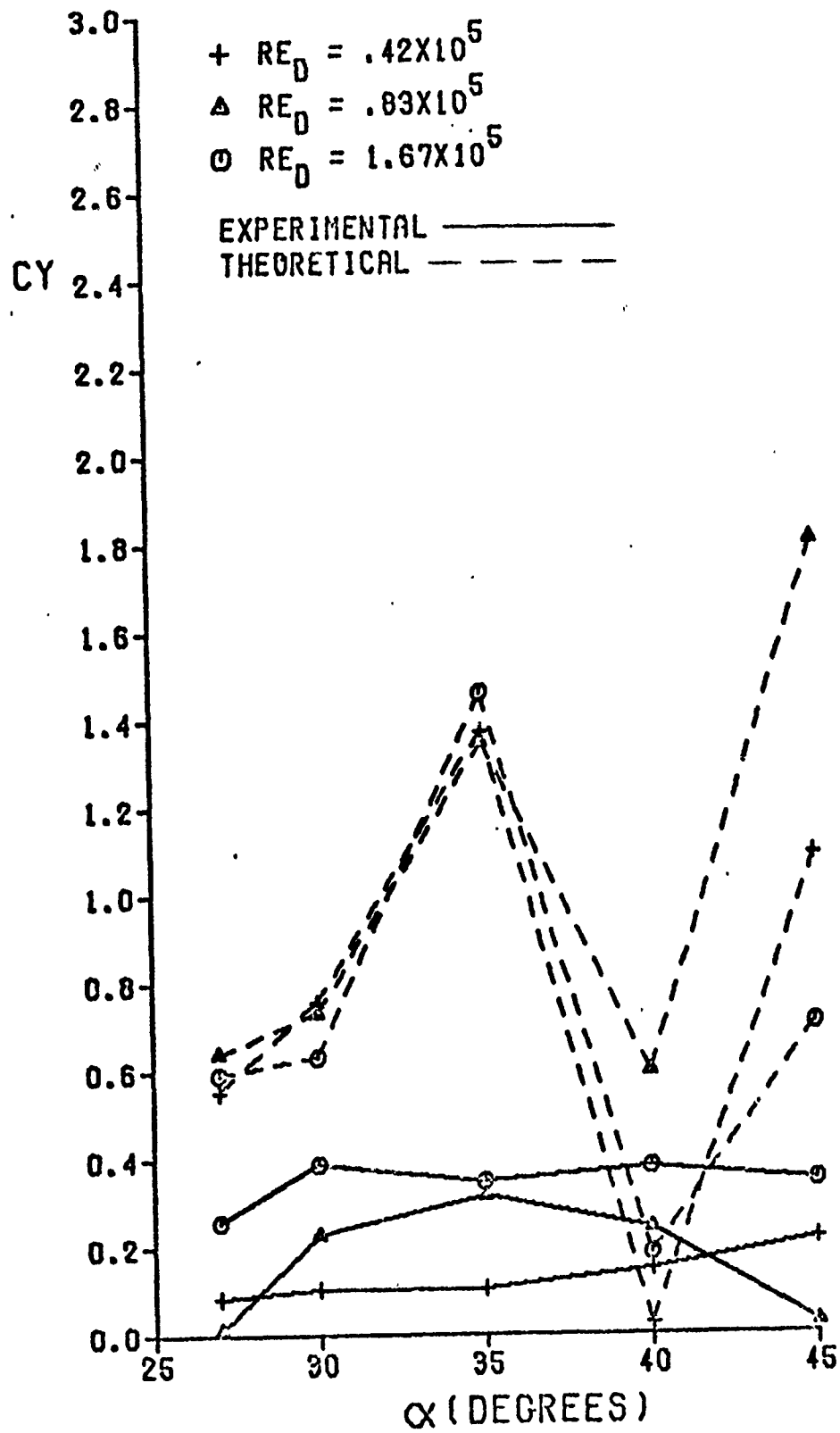


Fig 30. Local Side Force Coefficient at $M = .7$

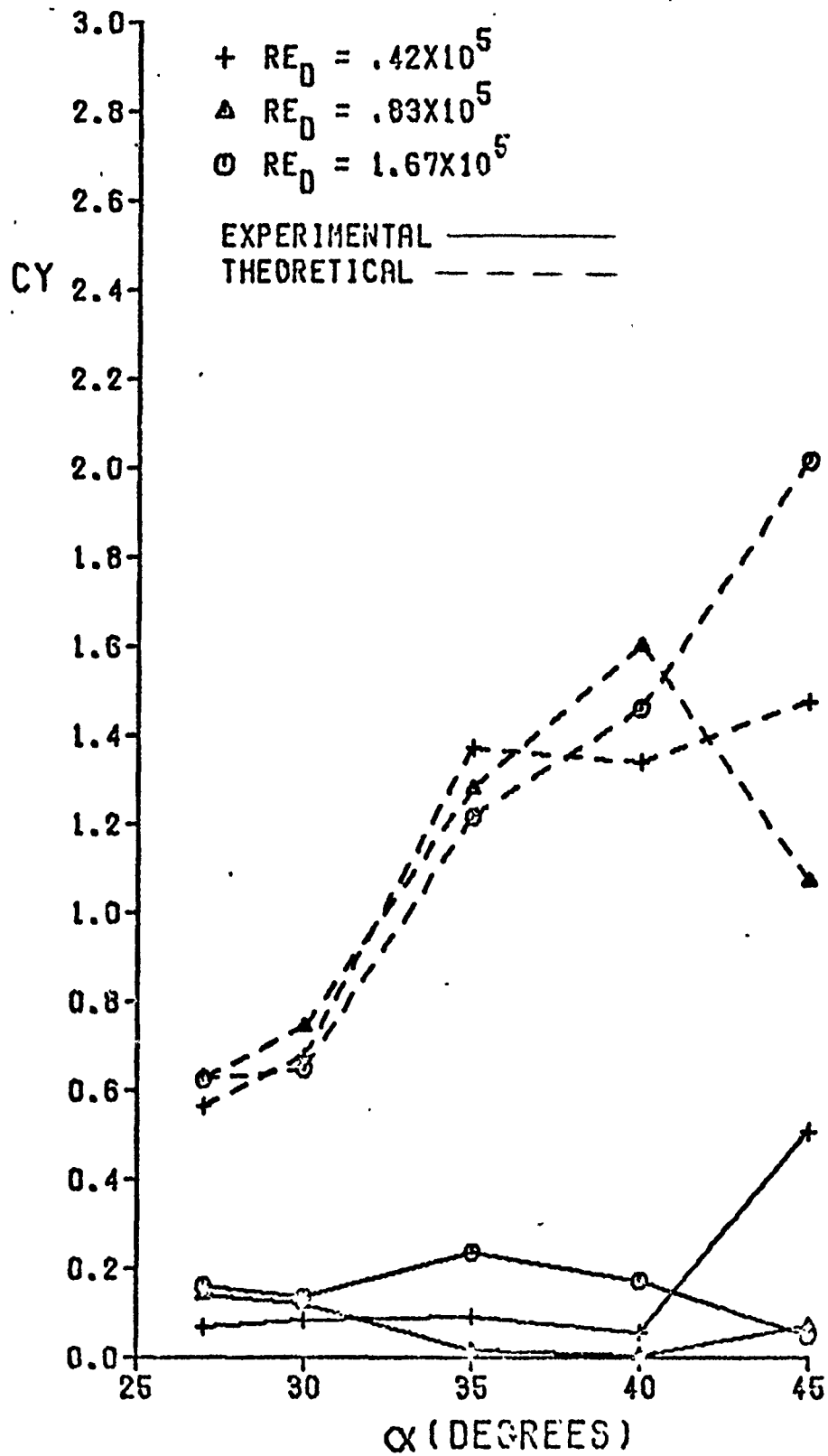


Fig 31. Local Side Force Coefficient at $M = .8$



Fig 32. Oil Flow at $Re_D = 41,667$, $M = .4$, $\alpha = 45^\circ$



Fig 33. Oil Flow at $Re_D = 83,333$, $M = .3$, $\alpha = 45^\circ$

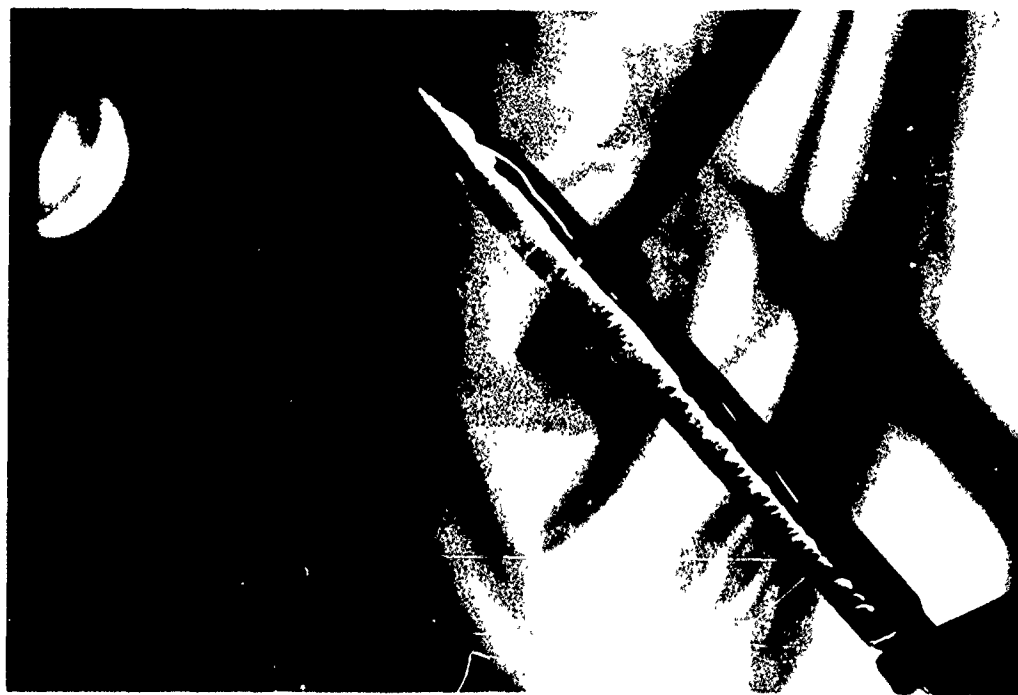


Fig 34. Oil Flow at $Re_D = 83,333$, $M = .6$, $\alpha = 45^\circ$



Fig 35. Oil Flow at $Re_D = 166,667$, $M = .3$, $\alpha = 30^\circ$

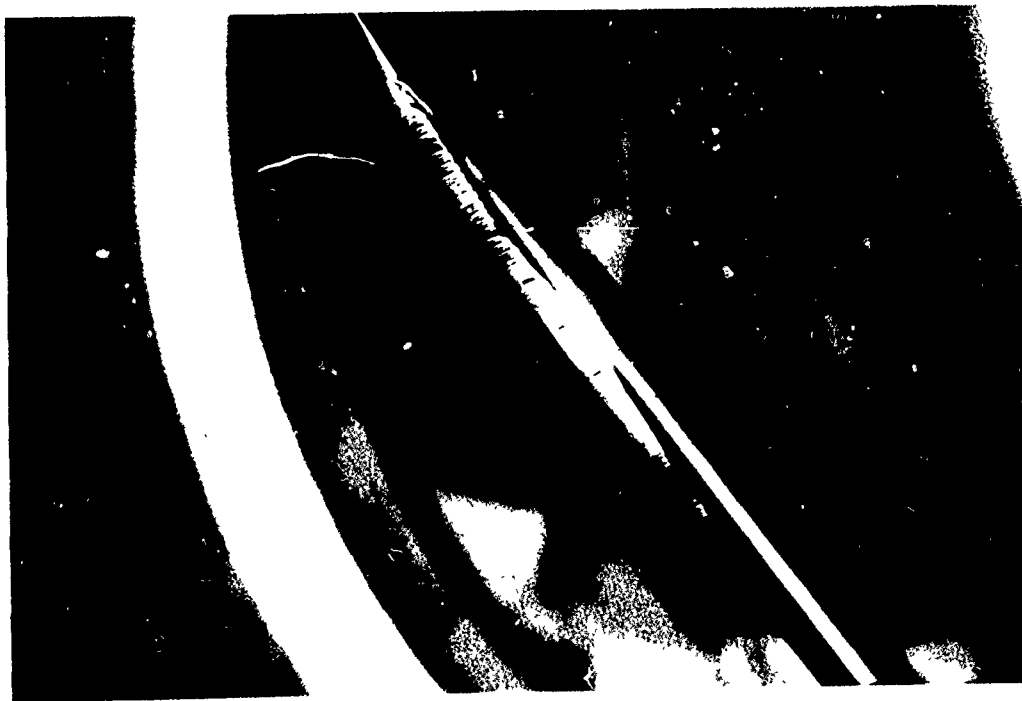


Fig 36. Oil Flow at $Re_D = 166,667$, $M = .3$, $\alpha = 45^\circ$

Bibliography

1. Kubin, J.S. An Analysis of Steady Asymmetric Vortex Shedding From a Missile at High Angles of Attack. Unpublished thesis. Wright-Patterson Air Force Base, Ohio: Air Force Institute of Technology, November 1973.
2. Prziembel, C.E.G. Aerodynamics of Slender Bodies at Angles of Attack - A Critical Review. AFFDL - TM -76 - 92 - FXG. Wright-Patterson Air Force Base, Ohio: Air Force Flight Dynamics Laboratory, August 1976.
3. Deffenbaugh, F.D. and Koerner, W.G. "Asymmetric Vortex Wake Development on Missiles at High Angles of Attack." Journal of Spacecraft, 14:155-162 (March 1977).
4. Flaherty, J.I. "Experimental and Analytical Investigations of High Angle of Attack Missile Aerodynamics." AIAA Paper No. 77-1156 (August 1977).
5. Lamont, P.J. and Hunt, B.L. "Pressure and Force Distributions on a Sharp-Nosed Circular Cylinder at Large Angles of Inclination to a Uniform Subsonic Stream." Journal of Fluid Mechanics, 76:519-559 (1976).
6. Reding, J.P. and Ericsson, L.E. "Maximum Vortex-Induced Side Forces on Slender Bodies." AIAA Paper No. 77-1155 (August 1977).
7. Wardlaw, A.B., Jr. "Multivortex Model of Asymmetric Shedding on Slender Bodies at High Angle of Attack." AIAA Paper No. 75-123 (January 1975).
8. White, H.L. Trisonic Gasdynamic Facility User Manual. Task Number 14760401. Wright-Patterson Air Force Base, Ohio: Air Force Flight Dynamics Laboratory, June 1973.
9. Baker, D.C. and Reichenau, D.E. Aerodynamic Characteristics of an MX Missile at Free-Stream Mach Numbers from 0.3 to 1.3 and Angles of Attack up to 180 Deg. AEDC-DR-99. Arnold Engineering Development Center, Tennessee, April 1975.
10. Thomson, K.D. and Morrison, D.F. "The Spacing, Position and Strength of Vortices in the Wake of Slender Cylindrical Bodies at Large Incidence." Journal of Fluid Mechanics, 50:751-783 (1971).

11. Dahlem, V.H., III. A Digital Computation Method for Determining the Hypersonic Aerodynamic Characteristics of Arbitrary Bodies. Task No. 136609. Wright-Patterson Air Force Base, Ohio: Air Force Flight Dynamics Laboratory, September 1962.
12. Fleeman, E.L. and Nelson, R.C. "Aerodynamic Forces and Moments on a Slender Body with a Jet Plume for Angles of Attack up to 180 Degrees." AIAA Paper No. 74-110 (February 1974).

VITA

Robert Rudolph Turelli, son of Mr. and Mrs. Robert Turelli, was born on 16 December 1949 in Highland Park, Illinois. He graduated from Carmel High School, Mundelein, Illinois in 1967 and attended Purdue University from which he received a Bachelor of Science Degree in Aeronautical and Astronautical Engineering in February, 1972. Upon graduation, he received a commission in the United States Air Force through the ROTC program and was assigned as a Deputy Missile Combat Crew Commander of a Minuteman II ICBM launch crew at Grand Forks Air Force Base, North Dakota. He progressed within three years to an Instructor Combat Crew Commander and in May, 1976 received the Air Force Commendation Medal. Through the Minuteman Education Program, he graduated from the University of North Dakota with a Masters Degree in Business Administration in August, 1976. He entered the School of Engineering, Air Force Institute of Technology, in June, 1976.

Permanent Address: 113 North Avenue
Highwood, Illinois 60040

This thesis typed by Diane Turelli

UNCLASSIFIED

SECURITY CLASSIFICATION OF THIS PAGE (When Data Entered)

REPORT DOCUMENTATION PAGE		READ INSTRUCTIONS BEFORE COMPLETING FORM
1. REPORT NUMBER AFIT/GAE/AA/77D-15 ✓	2. GOVT ACCESSION NO.	3. REPORTER'S CATALOG NUMBER <i>9 Master's thesis</i>
4. TITLE (and Subtitle) AN EXPERIMENTAL INVESTIGATION OF STEADY ASYMMETRIC VORTEX SHEDDING FROM A SLENDER BODY OF REVOLUTION AT HIGH ANGLES OF ATTACK.	5. TYPE OF REPORT & PERIOD COVERED MS Thesis	
6. AUTHOR(s) 10 Robert R. Turelli Captain USAF	6. PERFORMING ORG. REPORT NUMBER	
7. PERFORMING ORGANIZATION NAME AND ADDRESS Air Force Institute of Technology (AFIT-EN) Wright-Patterson AFB, Ohio 45433 ✓	8. CONTRACT OR GRANT NUMBER(s)	
9. CONTROLLING OFFICE NAME AND ADDRESS Air Force Flight Dynamics Laboratory Wright-Patterson AFB, Ohio 45433	10. PROGRAM ELEMENT, PROJECT, TASK AREA & WORK UNIT NUMBERS Project 1366 <i>16</i> <i>62201F</i> <i>1701</i>	
11. MONITORING AGENCY NAME & ADDRESS (if different from Controlling Office)	12. REPORT DATE <i>11</i> Dec <i>1977</i>	
	13. NUMBER OF PAGES <i>12264 p.</i>	
	14. SECURITY CLASS. (of this report) Unclassified	
15a. DECLASSIFICATION/DOWNGRADING SCHEDULE		
16. DISTRIBUTION STATEMENT (of this Report) Approved for public release; distribution unlimited.		
17. DISTRIBUTION STATEMENT (of the abstract entered in Block 20, if different from Report)		
18. SUPPLEMENTARY NOTES Approved for public release; IAW AFR 190-17 JERRAL F. GUESS, Captain, USAF Director of Information		
19. KEY WORDS (Continue on reverse side if necessary and identify by block number) Asymmetric Vortex Separation Missile Aerodynamics Side Forces On Slender Bodies Missiles at High Angles of Attack Normal Forces on Slender Bodies		
20. ABSTRACT (Continue on reverse side if necessary and identify by block number) An experimental investigation of the effects of Mach number and Reynolds number on the side forces induced on a slender body of revolution at high angles of attack was conducted. The tests were carried out in the Air Force Flight Dynamics Laboratory's Trisomic Gasdynamic Facility. The model tested consisted of a		

012225 Jmc

UNCLASSIFIED

SECURITY CLASSIFICATION OF THIS PAGE(When Data Entered)

sharp, tangent ogive nose of fineness ratio $L_N/D = 3.0$ followed by a cylindrical afterbody of fineness ratio $L_B/D = 7.5$. The model was tested at unit Reynolds numbers of 0.5×10^6 , 1.0×10^6 , and 2.0×10^6 per foot, Mach numbers between 0.3 and 0.8, and angles of attack between 27 and 45 degrees. From the pressure data, local side and normal force coefficients were calculated. These were compared to predicted local side and normal force coefficients using a current state of the art method. The results of the tests indicated that Mach and Reynolds numbers had a significant on C_N and C_Y . Increasing Mach number decreased the magnitude of C_Y , while increasing Reynolds number increased the magnitude of C_Y . The effect of Mach and Reynolds numbers on the magnitude of C_N depended on the particular flow conditions. No general trends were established. The predicted values of C_N and C_Y did not compare well with the values of C_N and C_Y obtained experimentally.

UNCLASSIFIED

SECURITY CLASSIFICATION OF THIS PAGE(When Data Entered)